



Norwegian University of
Science and Technology

Fluid Structure Interaction in a Pipe

Anders Thorstad Bø

Master of Science in Mechanical Engineering

Submission date: June 2018

Supervisor: Bjørnar Svingen, EPT

Norwegian University of Science and Technology
Department of Energy and Process Engineering

EPT-M-2018-17

MASTER THESIS

for

Student Anders Throstad Bø

Spring 2018

Fluid Structure Interaction in a Pipe

*Fluid-struktur interaksjon i et rør***Background and objective**

Through the Project work during the fall of 2017, the candidate has made a computer program that calculates Fluid Structure Interaction in a liquid filled straight pipe. The Method of Characteristics (MOC) was used to solve the so called Extended Water Hammer Equations. This solution methodology gives an almost analytical correct solution, under the constraints that the boundary conditions are taken care of 100%, and that the solution is within the limitations given by the method and modelling.

The objective of this master thesis is to continue this work. It is of special interest to verify the calculations. This should be done by experiments, but comparisons with other numerical solution techniques are also of interest. Eventual choices made here have to be scientifically substantiated, and also seen in relation to the available time.

If the student will go to Nepal for a excursion, earlier and further work will be presented as a publication and presented at the conference; 8th International symposium on Current Research in Hydraulic Turbines (CRHT-VIII) at Kathmandu University in March 2018.

The following tasks are to be considered:

- 1 Literature study about FSI, methods and verifications
- 2 Make a plan for the Master work
- 3 Work on the thesis
- 4 Eventual excursion to Nepal along with publication
- 5 Write a report

-- " --

Within 14 days of receiving the written text on the master thesis, the candidate shall submit a research plan for his project to the department.

When the thesis is evaluated, emphasis is put on processing of the results, and that they are presented in tabular and/or graphic form in a clear manner, and that they are analyzed carefully.

The thesis should be formulated as a research report with summary both in English and Norwegian, conclusion, literature references, table of contents etc. During the preparation of the text, the candidate should make an effort to produce a well-structured and easily readable report. In order to ease the evaluation of the thesis, it is important that the cross-references are correct. In the making of the report, strong emphasis should be placed on both a thorough discussion of the results and an orderly presentation.

The candidate is requested to initiate and keep close contact with his/her academic supervisor(s) throughout the working period. The candidate must follow the rules and regulations of NTNU as well as passive directions given by the Department of Energy and Process Engineering.

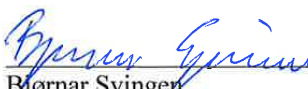
Risk assessment of the candidate's work shall be carried out according to the department's procedures. The risk assessment must be documented and included as part of the final report. Events related to the candidate's work adversely affecting the health, safety or security, must be documented and included as part of the final report. If the documentation on risk assessment represents a large number of pages, the full version is to be submitted electronically to the supervisor and an excerpt is included in the report.

Pursuant to "Regulations concerning the supplementary provisions to the technology study program/Master of Science" at NTNU §20, the Department reserves the permission to utilize all the results and data for teaching and research purposes as well as in future publications.

The final report is to be submitted digitally in DAIM. An executive summary of the thesis including title, student's name, supervisor's name, year, department name, and NTNU's logo and name, shall be submitted to the department as a separate pdf file. Based on an agreement with the supervisor, the final report and other material and documents may be given to the supervisor in digital format.

- Work to be done in lab (Water power lab, Fluids engineering lab, Thermal engineering lab)
 Field work

Department of Energy and Process Engineering, 15. January 2018


Bjørnar Svingen
Academic Supervisor

Research Advisor:

ABSTRACT

One of the recurring challenges concerning the development of fluid piping systems, is making them suitable for the task at hand. The system has to withstand all possible forces and motions associated with everyday use, as well as from more catastrophic one-time events. Nowadays, research efforts are being made to investigate how flexible power generation can be used to supplement other renewable, more unpredictable power sources like the wind and sun. Through this research, the need for hydraulic systems that are able to withstand several consecutive and rapid start-ups and shut-downs during a day becomes evident. Accurately depicting and studying these complex, transient events are more demanding, both computationally and experimentally, giving the need for specialized mathematical models and more task-specific instrumentation. Through project work during the fall of 2017 the candidate has made a computer program that simulates the fluid-structure interaction (FSI) in a liquid-filled, straight pipe. The mathematical model, the so-called extended waterhammer equations, are transformed with the method of characteristics (MOC), resulting in a numerical model capable of achieving an almost analytical solution to the set of equations.

The objective of this master's thesis is to conduct laboratory experiments with the aim of validating the calculations and verifying the theoretical background leading to the extended waterhammer equations. The experiments were conducted using an existing test-rig at the Waterpower Laboratory at NTNU. The transient measurements were done using miniature pressure transducers and linear strain gages placed at four different locations along the pipe length. All output signals from the rig were logged by a specialized program made with LabVIEW, and further processed in the programming language Python.

The results verifies the presence of the Poisson and junction coupling in the physical experiments. The validation process are more inconclusive, but the predictions are able to yield similar amplitude and wave propagation velocities as the measurement data in the first 0.5 seconds, but severely underestimates the first pressure and strain peak. Inaccuracies in the boundary condition-modeling and the forming of vapor cavities in the experimental rig are suspected to be among of the reasons why predictions fail to reproduce the measured system response.

SAMMENDRAG

En av de største utfordringene tilknyttet utvikling og dimensjonering av rørsystemer for væsketransport er å konstruere dem slik at de er egnet for sin spesifikke oppgave. Systemet må kunne motstå alle mulige krefter og bevegelser tilknyttet hverdagsbruken, samt takle sjeldne, men katastrofale hendelsene. Forsking blir for tiden gjennomført for å undersøke hvordan mer fleksibilitet i vannkraftproduksjonen kan supplere andre fornybare, men mer uforutsigbare energikilder, som for eksempel vind- og vannkraft. En slik utvikling vil føre til at hydrauliske system må være i stand til å motstå flere påfølgende og raske start- og stoppfaser i løpet av sin levetid. Evnen til å kunne studere og forstå disse komplekse, transiente hendelsene er krevende, både beregningsmessig og eksperimentelt, noe som gir behov for spesialiserte matematiske modeller og oppgavespesifikk instrumentering. Gjennom prosjektarbeid høsten 2017 har kandidaten skrevet et program som modellerer fluid-strukturinteraksjonen (FSI) i en væskefylt, rett rørlengde med en ventil i enden. Den matematiske modellen, den såkalt fire-likningsmodellen (the extended waterhammer equations), er transformert via karakteristikkmetoden (MOC) til en numerisk modell som presterer å gi en nesten analytisk løsning på problemet.

Denne masteroppgaven har til hensikt å gjennomføre et fysisk forsøk som søker å validere beregningene gjort med programmet og verifisere teorien som ligger til grunn for den matematiske modellen. Forsøkene er gjennomført på en eksisterende test-rigg ved Vannkraftlaboratoriet ved NTNU. De transiente målingene er gjort med miniatyrtrykkceller og lineare, foliestrekkklapper plassert fire forskjellige plasser på et rett rør. All eksperimentell data er logget gjennom LabVEIW og prosessert videre in programmeringsspråket Python.

Resultatene verifiserer at de ulike domenekoblingsmekanismene teorien forutser er tilstede i måledataene. Modellvalideringen er noe mangelfull, men den klarer å reproducere liknende amplituder og bølgeforplantningshastigheter som er funnet gjennom forsøkene, men kun for de første 0.5 sekundene av det transiente forløpet. Videre underestimerer beregningene den første trykk- og strekkbølgen i stor grad. Unøyaktigheter i grensebetingelsene i modellen, samt kavitasjonsbobler i røret under kjøring er mulige kandidater til å forklare avvikene mellom det som er observert og beregnet av den numeriske modellen.

ACKNOWLEDGMENTS

This work have been performed at the Norwegian University of Science and Technology (NTNU) as part of a 5-year master program in the field of Mechanical Engineering. It has been on the investigation and numerical modeling of the fluid-structure interaction in a pipe undergoing a waterhammer-event.

The work with this thesis has been an enormous learning-experience for me, allowing me to learn more about numerical modeling, practical programming and experimental analysis. It has had it's ups and downs, challenging me at every small turn. I've learned the hard way all that experimental studies usually provide speed-dumps on the way to the final result, forcing you back a step or two at a regular basis.

I wish to thank my supervisor, Bjørnar Svingen, for his guidance and his calm nature, which helped settle my nerves in the final stretches of completing this thesis. A thanks also to Joar Hilstad, all the help and guidance in the lab is much appreciated. I would also like to thank all students, ph.D candidates, post doctoral researchers, professors and staff associated with the Waterpower Laboratory at NTNU for creating an open-minded and relaxed environment where one can seek guidance in a time of need. It has been extremely helpful during my project work and master thesis.

CONTENTS

Abstract	i
Sammendrag	ii
Acknowledgments	iii
Table of Contents	vii
List of Tables	ix
List of Figures	xii
1 Introduction	1
1.1 FSI in General	1
1.2 Objective	2
1.3 Previous work	3
2 Theoretical Background	5
2.1 FSI-Effects in Pipes	5
2.1.1 Wave propagation and reflection time	6
2.1.2 Coupling mechanisms	7
2.2 Factors Influencing The Waterhammer	8
2.2.1 Water column separation	8
2.2.2 Two- and three-dimensional effects	8
2.3 Experimental Parameters and Calculations	9
2.3.1 Parameter calculations and conversion	9
2.3.2 Pressure measurement adjustment	11

2.3.3	The Wheatstone bridge	11
3	Experimental Setup and Procedure	13
3.1	Laboratory Setup	13
3.1.1	Physical setup	13
3.1.2	Instrumentation	15
3.1.3	Operating procedure	18
3.2	Uncertainty Analysis	19
3.2.1	Uncertainty in pressure transducer calibration	19
3.2.2	Uncertainty in pressure measurement	20
3.2.3	Uncertainty in strain measurements	21
3.2.4	Transient repeatability	23
4	Numerical Modeling	25
4.1	Simplifications and Assumptions	25
4.2	Domain Discretization and Physical Constant Modification	26
4.3	Boundary Conditions	28
4.3.1	Mass-spring-damper-model	28
4.3.2	Non-instantaneous valve closure	29
4.3.3	Challenges concerning new boundary conditions	31
5	Results	33
5.1	Experimental Results	33
5.2	Simulated and Experimental Response	38
5.2.1	Calculated variables	42
6	Discussion	45
6.1	FSI-effects	45
6.2	Model Validation	46
6.3	Model – Measurement Discrepancies	47
6.3.1	Experimental setup	47
6.3.2	Numerical modeling	47
7	Conclusion	49
7.1	Further Work	50
	Bibliography	51
	Nomenclature	55
A	Additional results	57

B	Uncertainty Analysis and Calibration	63
B.1	Relevant equations for the Uncertainty Analysis	63
B.1.1	Pressure measurements	63
B.1.2	Strain measurements	64
B.2	Pressure Transducer Regression Curves	65
C	Risk Assessment Report	67
D	CRHT-VIII Conference paper	73

LIST OF TABLES

3.1	Specification of L_i	14
3.2	Description of instrumentation.	15
3.3	Steady state conditions used for measurements.	18
4.1	Chosen variables to adjust the valve closure-equation	30
5.1	Model and experimental input-values for the simulation setup	38

LIST OF FIGURES

2.3.1 FBD of a cylindrical vessel under internal pressure.	10
2.3.2 A general diagram of a Wheatstone bridge circuit	11
3.1.1 Schematic of experimental rig.	14
3.1.2 Reservoir and pipeline seen from the upstream end.	16
3.1.3 Components at the downstream end.	17
3.1.4 Close-up of the instruments used for the dynamic measurements	18
3.2.1 Misalignment uncertainty visualized.	22
4.2.1 Characteristic lines in the stress-wave grid	27
4.3.1 FBD of a unrestrained, closed valve	29
4.3.2 Valve closure characteristic	31
5.1.1 Typical behavior at measurement-point A	34
5.1.2 Pressure-time behavior of the pressure transducers first 0.5 s	35
5.1.3 Strain-time behavior of the strain gages first 0.5 s.	36
5.1.4 Comparison of boundary conditions for the experimental rig.	37
5.2.1 Calculated response of the experimental setup	39
5.2.2 Measured pressure vs. simulated (free valve)	40
5.2.3 Measured strain vs. simulated (free valve)	41
5.2.4 Derived response of σ_z	42
A.1 Pressure-time behavior of the pressure transducers first 0.5 s	58
A.2 Pressure-time behavior of the pressure transducers first 0.5 s	59
A.3 Comparison of boundary conditions at points C and D.	60
A.4 Measurements against calculated response with a free, massless valve	61

A.5	Derived response of \dot{u}_z	62
B.1	Regression curves from calibration of the pressure transducers	66

CHAPTER 1

INTRODUCTION

One of the recurring challenges concerning the development of fluid piping systems, is making them suitable for the task at hand. The system has to withstand all possible forces and motions associated with everyday use, as well as from more catastrophic one-time events. The trade-off between cost and strength will then be one of key factors to take into consideration.

Nowadays, research efforts are being made to investigate how flexible power generation can be used to supplement other renewable, more unpredictable power sources like the wind and sun. These developments will result in hydraulic systems which need to be able to withstand several consecutive and rapid start-ups and shut-downs during a day. Decreasing ramp-up times will surely impose new challenges regarding oscillations and forces in and on the water-ways [1].

Accurately depicting and studying these complex, transient events are more demanding, both computationally and experimentally, giving the need for specialized mathematical models and more task-specific instrumentation. Adding the fact that to get an in-depth understanding of the entire system behavior, only considering the fluid parameters might not be enough.

1.1 Fluid-Structure Interaction in General

Fluid-structure interaction (FSI) can be defined as the coupled and dynamic interaction between fluid and structural subsystems. In general, this means that motion, forces and excitation will be translated between the different subsystems. Such systems can be objects immersed in a fluid flow field, such as a turbine blade, making the interaction external.

The opposite case is the internal FSI, which is that of a pipe conveying fluids or an artery transporting blood [2, 3].

The magnitude of this translation is heavily dependent on the type of system in consideration, which is what governs the coupling mechanism. If the domains are said to be strongly coupled, a change in one subsystem will yield a significant response in the other, which in turn alters the state of the first, indicating a strong dependency. A weak coupling can make it possible to account for interaction between the domains by simply adding the motion and forces from one domain to the other.

Investigation into the effects that originate from this dynamic coupling call for mathematical models capable of reproducing the complex behavior and mechanisms present. Two types of approaches can be followed. If both domains are modeled separately, using appropriate methods and equations, and an interface is added explicitly to translate the information between the fluid and structure, the approach is called partitioned.

If a model is developed treating the domains as one single system, a monolithic approach is chosen. These types of models have the interface implicitly incorporated in it's governing equations. The latter type has the advantage of translating information directly within the system. This is will give less room for numerical errors to affect the predictions. The partitioned approach, on the other hand, will most likely decrease development time because existing, well-proven models and computer codes can be used with only minor modifications [2].

1.2 Objective

The objective of this thesis is the verification and validation of a computer program which is used to described the fluid-structure interaction in a straight one-reach pipeline undergoing a waterhammer event.

This is to be accomplished through measurements done on an existing experimental setup at NTNU's Waterpower laboratory. Some additions and modifications to the experimental rig will be necessary to obtain results relevant to this thesis. Some modification will also be done to the computer program, with the aim of making the simulated and experimental case more equal. Specifically this will include applying a finer spatial mesh, incorporating non-instantaneous valve closure and adding a spring-mass-damper-system to the downstream boundary condition.

For further verification of the mathematical model, a more general study of FSI-mechanisms and relevant challenges in hydropower will be conducted. Relevant to this is the observation of the FSI-effects of precursor waves and junction coupling in the experiments.

1.3 Previous work

During the fall of 2017, the author wrote the computer program to be validated. It is written for the specific case of a waterhammer-event following the instantaneous closure of a simple valve. It is built on the extended waterhammer equations, which is a set of four partial differential equations, and the solution of this set using the method of characteristics (MOC). Preliminary validation of the program was done using a benchmark-case from Delft Hydraulics [4]. This showed promising results, but it is worth noting that the benchmark is strictly a virtual case.

Some observations of interest to take from the work done with the computer program is that the mathematical model is very sensitive to change in the boundary conditions and that the frictional and mechanical damping is practically non-existent.

THEORETICAL BACKGROUND

This thesis aims to investigate a straightforward and well understood fluid system, namely a reservoir-pipe-valve-system undergoing a waterhammer-event. Originally it consist of few and relatively simple components, but adding another layer by taking the fluid-structure interaction into account, introduces new effects and significantly alters the system behavior. The transition from numerical modeling to real-life experiment also introduce some new elements to consider. These factors will be presented in short here, as well as some relations needed for validating the numerical solution of the waterhammer-event, where the model response is to be compared with an experimental case.

2.1 Fluid-Structure Interaction-Effects in Pipes

For pipelines in general, the most notable FSI-mechanism occurs when the system experiences a rapid change in fluid velocity and is usually denoted a pressure surge¹. Traditionally, these types of events have been treated as a strictly transient, fluid problem, solved using the continuity and momentum equation. Consequently, the surrounding structure has been considered rigid, unable to influence or be influenced by the pressure fluctuations inside the pipe. Since most materials used for conveying fluids will exhibit an elastic behavior when exposed to a force, that assumption is not entirely correct. Taking pipe-wall elasticity into account makes the problem dependent on the FSI between the fluid and pipe-wall.

¹ The term waterhammer is often used when considering hydraulic systems.

2.1.1 Wave propagation and reflection time

The information traveling through the system is governed by the propagation of two different acoustic waves, a pressure wave and axial stress wave. The unrestrained wave propagation velocity can be determined using the general relationship

$$c_i = \sqrt{\frac{B}{\rho_i}} \quad (2.1)$$

where B and ρ_i is the bulk modulus and mass-density of the medium in question [5]. For the two respective media for FSI-applications, B will be taken as Young's modulus, E , for the pipe-material and the fluid elastic modulus, K .

Furthermore, the pressure wave will be influenced by the surrounding structure, and actually slowed down, due to the constraint put on it. The relationship giving the restrained pressure wave propagation velocity can be found as

$$c_f = \sqrt{\frac{K}{\rho_f} \left(1 + \psi \frac{DK}{eE} \right)^{-1}} \quad (2.2)$$

The ψ in the above equation account for the amount on restraint put on the system with respect to anchoring (see [6, Ch.2]). It can be assumed, for most real-world applications, that the axial stress wave, c_s , will be significantly faster than the pressure wave, c_f , due to the differences in physical constants. One important note is that there exists other wave modes, but the pressure and stress wave are the dominating ones when long wavelengths are assumed² [4]. An effect that c_s can experience is when it comes in contact with pipe-fittings and anchoring points. These can in fact act as reflective surfaces for c_s , effectively shortening the pipeline felt by the axial stress waves [7].

Relevant for the study of waterhammer effects is the pressure wave reflection time. As the transient is initiated, the sudden change in fluid pressure creates a wave traveling upstream with the velocity c_f . When the wave reaches the upper reservoir, all kinetic energy is lost and the fluid is brought to rest. The constant pressure in the reservoir forces the fluid to flow again and the wave travels downstream, returning the pressure back to the original state. When it reaches the downstream end, the wave have now traveled two times the pipeline length. The wave reflection time can then be expressed as

$$t_{c_f} = \frac{2L}{c_f} \quad (2.3)$$

The reason this is an important system parameter, is that it indicates one of the transient time-scales for the waterhammer. If the mechanism initiating the event is instantaneous

² The wavelengths are considered long compared to the radius of the pipe.

valve closure, the pressure wave is again reflected, because of the zero-discharge boundary condition at the downstream end [6]. More relevant for real-life applications is where the valve closure-time, $t_c \neq 0$. This gives two cases, namely:

1. $t_c \leq t_{cf}$: This condition ensures zero discharge at the instant where the pressure wave returns, and no energy is lost through the valve opening. This gives a reflected wave with approximately the same strength as it started out with.
2. $t_c > t_{cf}$: Here, the fluid will have fluid velocity, $V \approx V_0$, meaning that a small amount of fluid will escape through orifice left by the incomplete closure of the valve and energy is lost. The result is a slightly weaker wave, depending on the amount of energy lost through the valve. If $t_c \gg t_{cf}$, too much may be lost in the reflection process and the waterhammer dies out.

2.1.2 Coupling mechanisms

Three coupling mechanisms are assumed to exist with respect to a fluid-pipe-system, the junction, Poisson and friction coupling. They all make some contribution to the FSI-effects, but the two first have the largest impact on the overall behavior. The latter seeks to describe the friction forces arising due to the no-slip boundary condition between a viscous fluid and pipe-wall. Of the three couplings, it's effect diminish in comparison to the other two, especially for rapid, short-lived transient events.

The Poisson coupling is present in the system because of the material contraction factor, ν . A change in pressure will result in a change in pipe cross-sectional area. As a result, an axial stress wave will propagate in front of the initial pressure wave. The radial change of the pipe-wall will cause an equal, but opposite change in the adjacent structure due to ν . Since the internal pressure inside the pipe depends on the felt cross-sectional area, it will also change, producing another pressure wave in-front of the original. This is known as the precursor wave and is a faster, but weaker pressure wave. In fact, the theory that the presence of the precursor builds on finds its propagating velocity to be approximately that of the axial stress wave. It is suspected to be present in calculations and physical experiments as a small disturbance in the overall behavior [7, 8]. The ν is a measure of the transverse contraction to longitudinal extension when a specific material is subjected to a force in the longitudinal direction and is often called the Poisson's ratio. For the system to be fully decoupled this factor must be strictly put to zero, because it will mean no reaction to an applied force, i.e. a material that is strictly rigid. For all real-life applications, it can be safely assumed that $\nu \neq 0$ and $\nu > 0$ [9].

The junction coupling explains mechanisms concerning specific points in the system, such as at bends, straight connections and terminal points³. Assumed that the system is allowed to move, the internal forces acting on a closed valve or pipe-bend will result in

³ Terminal points can be defined as pipe-components other than the pipe itself, such as valves, reservoirs, pumps and turbines.

opposite and mutual forces inside the pipe wall, adding another dynamic component to the system behavior. Different from the two previous coupling mechanisms, which act on the entire pipe-reach, this will only be present at the junctions. It is also considered to be the mechanism that gives the most significant FSI-effects of the three [4].

2.2 Factors Influencing The Waterhammer

All real-life events experience effects from the environment around them that directly influence their behavior. During a pressure surge, the type of fluid, properties of the surrounding pipe and the fact that physical phenomena exist in three-dimensional space will force the event to play out in a certain way. A general understanding of how these factors influence the waterhammer is needed to aid in the verification and validation process of the numerical model and will be addressed in short here.

2.2.1 Water column separation

When a fluid pipe-system undergoes a surge, the resulting pressure response can be so significant that it drops all the way down to vapor pressure. If this happens, cavitation or a water column separation may occur. The former can be defined when the cavitation come in the form of dispersed, small bubbles of vapor, while the latter happens when larger bubbles form at specific points or sections of the pipe. For horizontal pipes, this separation tend to form a thin cavity on the top of the pipe and may stretch out axially [10, Ch.9].

The presence of such cavities will affect the system behavior. The bubbles will expand or contract due to the changes in pressure, causing energy from the pressure wave to dissipate into thermal energy. The cavities will also dampen out the waterhammer-effects by slowing down the wave propagation velocity [10, Ch.9].

2.2.2 Two- and three-dimensional effects

Another factor which will play a part in the real-life transients is the fact that the event exist in three-dimensional space. Considering a cylindrical coordinate-system, the three coordinates will be denoted r , ϕ and z , as the radial, circumferential and axial coordinate. For pipe-flow, this can be simplified more be stating that the flow can be taken as symmetric about the the pipe's central, z , axis. But the domain is still two-dimensional, with variations in both pressure and velocity along the r - and z -axis, respectively.

The numerical model used to describe a pressure surge in this thesis uses a one-dimensional assumption, averaging the fluid and structural variables over their respective cross-sectional areas⁴. This averaging now neglects any radial change of the velocity in the pipe. Physically, this is inaccurate because of the no-slip condition, giving a parabolic-shape to the velocity profile.

⁴ The model and it's specifics will be addressed further in a subsequent chapter (Chapter 4)

The boundary condition gives rise to friction between the fluid and the surrounding structure, forcing the fluid to a rest at the pipe-wall. In steady pipe-flow, the frictional forces can easily be derived by a control-volume analysis, relating the shear stresses to pressure loss, giving

$$\tau_0 = f \frac{\rho_f V_0^2}{8} \quad (2.4)$$

where τ_0 is the steady shear stress, f is the system friction factor and V_0 the average fluid velocity[4]. Traditionally, this expression has been used extensively in waterhammer-modeling, mostly due to it's ease-of-implementation and that the shear stresses are assumed to experience little to no change in the first few moments of the transient. Although this is one of the more popular approaches to model friction, the steady assumption is not able to provide sufficient damping to the fluctuations, especially struggling to attenuate the first few pressure peaks following transient initiation [11]. Unsteady friction models are therefore suggested to account for the additional losses due to the two- and three-dimensionality introduced by the velocity profile [12].

Another effect of the one-dimensional model, is that the pipe-motion is assumed to be restricted to the central axis as well, and comes from the dominating wave-modes in the system (see section 2.1.1). As a pipeline is excited by a change of pressure, both axial stress and pressure waves start propagating through the system. Considering a general pipeline, bends, anchoring-points and other elements will be affected by these waves, as well as affecting the waves themselves. If the bend is allowed to move or anchoring-points are flexible, the fluctuating forces and velocities may cause two- and three-dimensional motion. In addition to increasing the danger for pipe-failure, these off-axis motions also draw energy from the system, significantly altering the response [13].

2.3 Experimental Parameters and Calculations

The experiments that were conducted as a part of this thesis acquired data from direct measurements of two parameters, namely fluid pressure and pipe-wall strain. Using existing relationships, estimates of other parameters of interest can be accessed and used in when evaluating the data. Specifically, the relations used here will be the strain-displacement-relation and thin-walled pressure vessel theory. The sensing principle of the Wheatstone bridge will also be addressed. Understanding this proved to be important for the post-processing and uncertainty analysis of the strain measurements.

2.3.1 Parameter calculations and conversion

One of the parameters of interest is the stress-components inside the pipe-wall during the transient. Generally for thin-walled, cylindrical vessels, there is a state of planar or biaxial stress, meaning that stresses in the radial direction can be neglected ($\sigma_r \rightarrow 0$) [15]. The

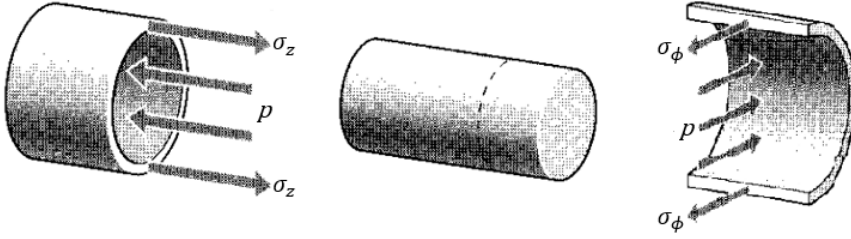


Figure 2.3.1: Free-body-diagram of a cylindrical vessel under internal pressure, p [14].

two other stresses present in the system are the axial and circumferential components, σ_z and σ_ϕ . Evaluating a force-balance of the free-body-diagram (FBD) of a pressurized cylindrical vessel in figure 2.3.1, will yield

$$\sigma_\phi = \frac{r}{e} p \quad (2.5)$$

Here, r and e represent the pipe internal radius and pipe-wall thickness, respectively. An important requirement of the above expression is that the system is closed off at the ends [14]. It is also worth noting that the theory used is for the equilibrium state of such a system. Using the expression for a transient problem are only assumed to give a rough estimate of σ_ϕ . An expression for σ_z can be found by using the stress-strain-relation (see equation (B.6)). Solving it for the axial stress gives

$$\sigma_z = E\varepsilon_z + \nu\sigma_\phi = E\varepsilon_z + \frac{r}{e} p \quad (2.6)$$

The above relationship was also used in the derivation of the extended waterhammer equations, and can therefore be seen as a suitable approximation of the axial stresses.

Relating pipe-wall displacement to strain comes directly from the strain-displacement-relation. In the axial direction, z this is given by

$$\varepsilon_z = \frac{\partial u_z}{\partial z} \Leftrightarrow u_z = \int_0^z \varepsilon_z dz \quad (2.7)$$

where the right expression is the relation solved for the displacement, u_z [4]. Differentiating this with respect to time, the displacement velocity of the pipe-wall can be obtained as

$$\dot{u}_z = \frac{\partial u_z}{\partial t} \Rightarrow \dot{u}_z = \frac{\partial}{\partial t} \left(\int_0^z \varepsilon_z dz \right) \quad (2.8)$$

For the transient case under investigation here, all structural and fluid parameters are time-dependent. If the integral in equation (2.7) is evaluated between points (z_1, z_2) , the dis-

placement velocity in the system can be found as

$$\dot{u}_z = \frac{\partial}{\partial t} \left(\int_{z_1}^{z_2} \varepsilon_z dz \right) = \frac{\partial}{\partial t} \left[\varepsilon_z z \right]_{z_1}^{z_2} \quad (2.9)$$

or

$$\dot{u}_z = (z_2 - z_1) \frac{\partial \varepsilon_z}{\partial t} \quad (2.10)$$

This can be used to access estimates of \dot{u}_z by using the technique of finite differences, which is a common way of numerical differentiation [16, Ch.2.5].

2.3.2 Pressure measurement adjustment

The transducers used to measure fluid pressure have their sensing elements mounted flush with the internal pipe-wall. This means that the output gives information of the pressure at a point at the wall, not the centerline, making it necessary to adjust the output to obtain a prediction of the fluid pressure at the system centerline. This is wanted because the calculated pressure-value represents the averaged pressure over the fluid cross-sectional area. The adjustment will be done by calculating the hydrostatic pressure at the centerline, seen from the top of the pipe, where the transducer is placed.

2.3.3 The Wheatstone bridge

One of the most common and convenient ways to do strain measurements is using strain gages. They use the fact that the resistance, R , in thin metal wires or foils change as a function of the tension put on them. Arranging the gages in a circuit, allows the user to convert this change in resistance to a voltage, and consequently a strain reading. The arrangement used for the experiments conducted as a part of this thesis are known as the Wheatstone bridge. A general circuit-diagram can be seen in figure 2.3.2. When mounted on a specimen, one or more of the R_i are represented by a strain gage giving a quarter, half or full bridge-configuration. Here, the quarter-bridge is used, with one active and one

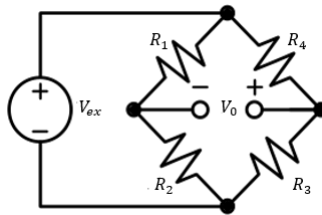


Figure 2.3.2: A general diagram of a Wheatstone bridge circuit [17].

dummy resistance⁵ [17]. The signals read from the bridge-circuit are given in terms of a change of voltage, U_R . Accessing the strain, which is a relative elongation from an original state given by

$$\varepsilon_i = \frac{\Delta L}{L_0} \quad (2.11)$$

the following relationship can be used

$$\varepsilon_i = -4U_R \left(\frac{R_G + R_I}{R_G G(1 + 2U_R)} \right) \quad (2.12)$$

where R_G and R_I are the gage and lead-wire resistance of the bridge, G is the gage-factor. U_R are the relative voltage output of the bridge and can be found as

$$U_R = \frac{U - U_0}{U_{ex}} \quad (2.13)$$

where U and U_0 is the strained and unstrained voltage output, while U_{ex} is the bridge excitation voltage [17].

⁵The dummy resistance is used for circuit-completion and is a simple resistor with the $R = R_G$

CHAPTER 3

EXPERIMENTAL SETUP AND PROCEDURE

In order to properly validate the mathematical model and simulation results, an experimental rig capable to initiate and measure a waterhammer-event was needed. Given that the waterhammer is dynamic, fluctuating and very rapid, extra care had to be taken in the setup and execution of the experiment. An existing pipeline at the Waterpower Laboratory at NTNU, formerly used for Pelton-turbine testing, was repurposed for this thesis. Some minor modification were then necessary when considering the FSI-aspect, where structural movement also was of interest.

3.1 Laboratory Setup

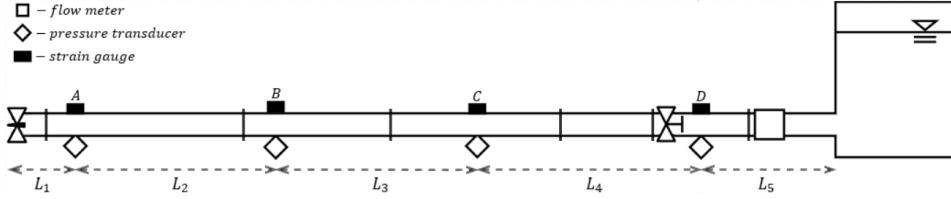
The nature of a pressure surge is chaotic and fast, with high frequency fluctuations, especially in the structural domain. Due to this, a few criteria of importance had to be met by the experimental rig. Considering the constraint with pressure wave reflection time (see section 2.1.1), it can either be overcome with the appropriate choice of pipe length or a valve with a satisfactory closure-time. Another criterion is the pipe-wall thickness, mainly since the mathematical model assumes a thin-wall structure. This will be especially important when conducting the experiment, because a thin-walled structure makes the assumption of no radial stresses mathematically valid. Lastly, instrumentation capable of tracking the rapid fluctuations produced by the waterhammer will be crucial to get valuable measurement-data out of the rig.

3.1.1 Physical setup

The choice of pipe length and wall-thickness were fixed because an existing pipeline was used. A schematic of the setup can be found in figure 3.1.1. The pipe has a total length

Table 3.1: Specification of L_i in figure 3.1.1

L_i	L_1	L_2	L_3	L_4	L_5
Length [mm]	990	6070	6010	6130	5000

**Figure 3.1.1:** Schematic of experimental rig, where water flow from right to left. Black lines across the pipe indicates the anchoring points for the pipe.

$L = 24200$ mm, an inner diameter $D = 100$ mm and a wall thickness $e = 2$ mm. The upstream reservoir is a high pressure tank with a free water surface, and is fitted with a gage showing the air pressure above the free surface. The downstream valve is a Pelton nozzle with an outlet diameter of $d = 40$ mm. The inclination angle between the reservoir and nozzle is approximately zero. The upstream valve is a manual butterfly valve in place to shut off the water supply to the pipe when it is not in-use. Furthermore, the pipe is designed to endure an internal pressure of $P_* = 10$ bar, which will be the upper limit for the experiments.

The pressure tank has a constant water-supply from a centrifugal pump, drawing water from a large reservoir in the basement of the laboratory. The pump was to be used to control the volume flow and reservoir pressure as the fluid input values for the system at steady state. The tank has an escape valve, which when closed, helps keep the free surface-level height inside approximately constant for different pressure heads.

The existing pipeline have a Pelton nozzle fitted at the downstream end. The needle position was operated manually with a lever mounted on top of the nozzle body, reaching out the top of the chamber (see figure 3.1.3b). This was seen as a quick and easy way to modify the closing mechanism to fit the needs for the measurements. The first tests conducted proved it sufficient to produce a pressure surge, even though the closing time was found to be up to four times greater than the theoretical wave reflection time.

The discharge chamber (see figure 3.1.3a) encasing the nozzle is bolted to the laboratory floor, presumably restraining most of the nozzle movements. Originally, the downstream end of the pipe was fixed to the chamber as shown in figure 3.1.3d. The plate where the pipe enters the chamber was taken away, giving the possibility to investigate the free-valve boundary condition, which is important with respect to investigation of the junction coupling (see section 2.1.2). The pipe is also anchored to the laboratory-floor using two-legged saw-horses and clamps to anchor the pipe rigidly. The clamps were loosened for some of the measurements, to see if this gave an observable change to the system response.

Table 3.2: Description of instruments used for the measurements.

Variable	Limit	Instrument	Calibration
Pressure	17 bar	Kulite HKM-375M-17BARA	DPI 601
Strain	$\pm 5\%$	HBM LY19-10/120A	Null offset
Acceleration	25 kHz	B&K DeltaTron Type 4397	Factory calibration
Flow	100 l/s	Krohne Optiflux 2300C	–
Nozzle position	2000 mm	ASM Model WS17KT 2000	–

I/O Modules	Input range	Sample rate	Chassis
NI-9237 (Bridge)	± 25 mV/V	51.2 kS/s/ch	NI-9178
NI-9233 (IEPE)	± 5 mV/V	50.0 kS/s/ch	NI-9178

3.1.2 Instrumentation

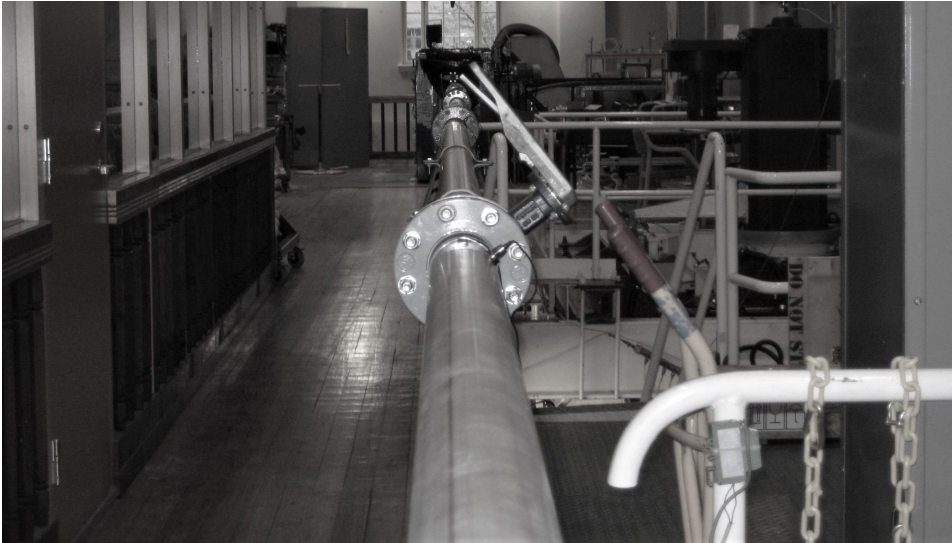
The instrumentation used for tracking the dynamic change of the system state need to have a response time that can match the fluctuations of the system variables. Another demand is that they need to be sensitive enough to notice small changes as both regular and precursor waves propagate through the system media at different velocities.

The dynamic measurements were done using miniature pressure transducers, strain gages and single-axis accelerometers at four different locations along the pipe. These correspond to point A-D in figure 3.1.1. The sensors measuring both pressure and strain are bridge-based sensor, where the transducer has a full bridge sensing element. The strain gages used was linear, metal-foil gages, mounted to measure axial elongation and contraction in a quarter bridge-configuration, with 120Ω dummy resistance attached offset of the gage. The pressure transducer is mounted on the outside of the pipe so that the sensing element is positioned flush to the inner pipe-wall. The sensors used for pipe acceleration measurements¹ uses piezoelectric elements and were mounted on stubs on the pipe-flange, with the active axis along the pipe.

In addition to the main sensors, one electromagnetic flow-meter and one string-potentiometer have been used to monitor stationary flow rate and nozzle position during the experiments. This helped determining the appropriate initial conditions and nozzle characteristics in the validation-process. The instruments and cDAQ-modules used, together with their specifications, are listed in table 3.2.

All output signals from the rig were logged by a specialized program run through LabVIEW. It was made to be lightweight and easy-to-use, so most processing of the signals were therefore done afterwards using a computer program written in the same programming language as the MOC-computer program, Python. This also made comparison of experimental and simulation data easier.

¹ Only one accelerometer was eventually used, placed at point B, mainly due to supply and available time.

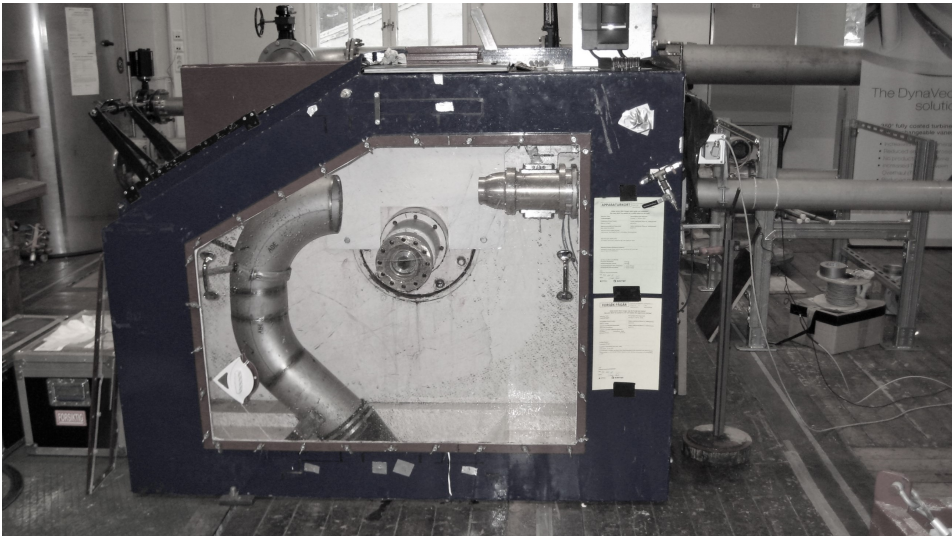


(a) Entire pipeline, seen from upstream.

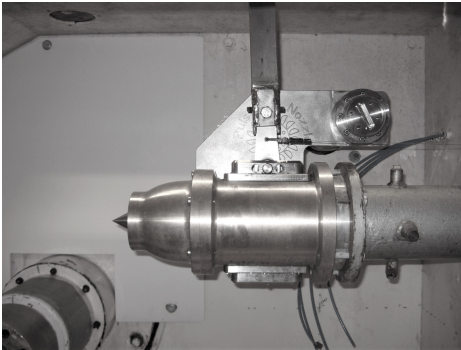


(b) Close-up of the top of the pressure tank, pipeline seen emerging at the middle of the picture.

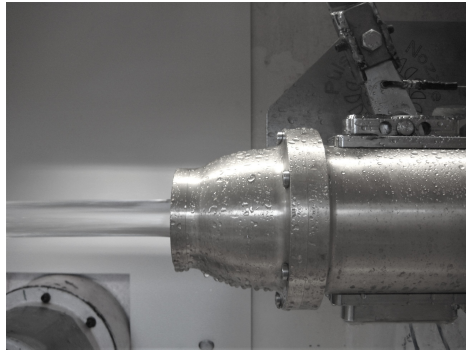
Figure 3.1.2: Reservoir and pipeline seen from the upstream end.



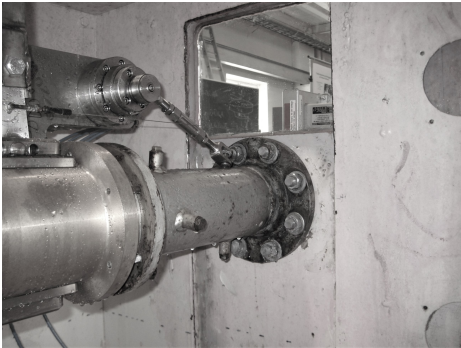
(a) Discharge chamber.



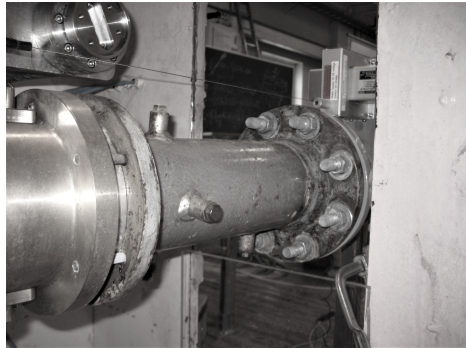
(b) Pelton nozzle, closed.



(c) Pelton nozzle, open, with water flowing.



(d) Rigidly fixed valve to chamber.



(e) Valve decoupled from chamber, free to move.

Figure 3.1.3: Different components at the downstream end of the pipeline.

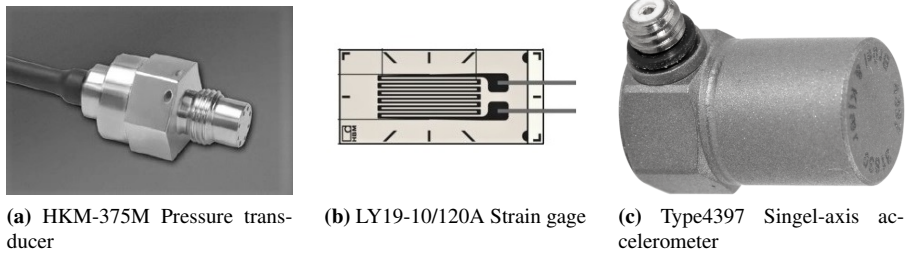


Figure 3.1.4: Close-up of the instruments used for the dynamic measurements [18, 19, 20].

3.1.3 Operating procedure

In order to make every measurement series as equal as possible, a standard procedure was followed. The pressure tank was first filled to about 89% of total capacity, which gave approximately one meter of water behind the upstream inlet. After closing the escape valve, the reservoir pressure and volume flow in the pipe was controlled using the pump rotational speed. Following the start-up procedure, the rig was run with a constant volume flow for ten minutes to ensure a steady state and no entrapped air in the pipe. Since strain gages also are sensitive to change in temperature, this also allowed the pipe to cool down to a more steady temperature, giving more stable readings from the gages.

The general procedure for measuring the transient behavior of the setup consisted of initiating the computer program, moving from the work station to the discharge chamber, pulling the lever and keeping the nozzle closed for five to ten seconds. Given that the first, few moments of the waterhammer are the most interesting, at least for this study, this was deemed sufficient. After releasing the lever again, the rig was allowed at least two minutes to settle before another transient measurement was taken. When the initial conditions were altered, the rig was again run constantly for at least five minutes to allow the new steady state to be reached. Measurements were taken with four different volume flows, the specifics can be found in table 3.3. At least three series were obtained at each flow rate. Since the phenomenon under investigation are transient, the repeated measurements were meant to check repeatability of the results.

The manual operation of the nozzle’s lever added some unwanted effects and distur-

Table 3.3: Steady state conditions used for measurements.

Reservoir head[mWc/bar]	Flow rate / velocity[m ³ /s]/[m/s]	Pump rotational speed[RPM]
3.85 / 0.3750	0.0057 / 0.726	377.0
4.75 / 0.4622	0.0068 / 0.866	397.0
5.65 / 0.5495	0.0077 / 0.980	417.0
6.65 / 0.6464	0.0086 / 1.095	437.0

bances due to the human interaction with the rig. The operator of the rig was the one closing the nozzle to initiate the transient. It is therefore safe to assume that there was some inconsistency in closure-time. The setup also demanded passing in close proximity to the pipe when moving from the work station to the discharge chamber. During the first tests of the setup, it was observed that this disturbed the strain-readings at measurement-points A and B. The problem was easily omitted by postponing the waterhammer-initiation, allowing the system to settle back again. Lastly it was noticed during tests with the free nozzle that holding the lever too tight restrained the nozzle-motion, which again results in unwanted disturbances of the system in the measurement-interval.

Risk assessment

During the planning of the experiments, a risk assessment was conducted for the rig. This is a requirement from the department² when new activities are planned in the laboratory. This experiment deals with water as it's working medium, at fairly low pressures and volume flows, so only a few minor hazards were identified. Although the pressure is low in steady state, purposely initiating a waterhammer will give a significant increase. The pipeline, with pipe and all fittings, are designed to withstand $P_* = 10$ bar, so a pipe-burst was seen as possible, but unlikely. Other hazards considered were harm from large pipe motion and minor water-leakages from bad fittings. The full risk assessment-report can be found in the digital attachment associated with this thesis.

3.2 Uncertainty Analysis

All experimental activity and data acquisition are subject to errors associated with the measurement process or the sensors and instruments used. They can originate from inaccuracies in the sensors themselves, human interaction or the environment around where the setup is located. Quantifying these is an important aspect of experimental studies, because the uncertainty of a measurement process gives indications to whether or not the measured value can be attributed to the process under investigation. This section addresses the specific uncertainties for each of the instruments used for the dynamic measurements. This analysis is based on theory given in [21], and the specifics about the errors and calculations can be found in appendix B. For all sources listed below, e_{x_i} and f_{x_i} will denote absolute and relative uncertainty, respectively.

3.2.1 Uncertainty in pressure transducer calibration

There are three relevant types of errors which must be accounted for in the pressure transducer calibration. Those are the systematic and random uncertainties in the calibrator itself, e_{P_a} and e_{P_b} , and the repeatability error in the transducer (also known as the regression error), $e_{P_{reg}}$

² Department of Energy and Process Engineering, NTNU

Calibrator: The method used to calibrate the pressure transducers was with a digital pressure indicator (Druck DPI 601). It's documentation states that it has an accuracy of $f_{P_{a,b}} = \pm 0.05\%$ of FSO³.

Regression: From the calibration, the uncertainty from the curve-fit is estimated using the data available in the calibration reports found in the digital attachment of this thesis. The regression curves for each transducer can be found in figure B.1. Regression analysis of this gives a representative uncertainty due to regression as $f_{P_{reg}} = 0.002734\%$. This was calculated using a t -distribution-approach on measurements for ten different steady state-series, using equation (B.1).

A common way to estimate the combined uncertainty of a process or quantity is to use the root-mean-square (RSS)-method, given as

$$e_q = \left[\sum_{i=1}^n (e_{q_i})^2 \right]^{1/2} \quad \text{or} \quad f_q = \left[\sum_{i=1}^n (f_{q_i})^2 \right]^{1/2} \quad (3.1)$$

where subscript q_i is the uncertainty from error component i [21]. From the calibration of the pressure transducers, the RSS-method gives

$$f_{P_{cal}} = \left[(f_{P_{reg}})^2 + (f_{P_{a,b}})^2 \right]^{1/2} = 0.05191\% \quad (3.2)$$

As seen from the value of $f_{P_{cal}}$, the accuracy of the calibrator itself has the largest impact on the total calibration uncertainty. This is to be expected because that instrument is what decides the input the sensor receive. Any drift or irregularities in the input-signal will therefore directly influence the recorded output during calibration. The uncertainty can be lowered, if seen as necessary, by using more accurate and stable calibration-equipment.

3.2.2 Uncertainty in pressure measurement

For the measurement process, four different sources of error can be identified. The combined uncertainty from the calibration must be taken into account, $e_{P_{cal}}$, together with additional systematic and random uncertainties in the transducer, e_{P_h} and e_{P_j} , and some uncertainties in the physical properties, e_{P_l} .

Pressure transducer: The systematic uncertainty associated with the pressure measurements depends on the instruments hysteresis, nonlinearity and repeatability. All these combined can be found in the data sheet as $f_{P_h} = \pm 0.1\%$ of FSO ($e_{P_h} = \pm 0.017\text{bar}$). Furthermore, analysis of the steady state behavior of the sensors gives a random uncer-

³ FSO - Full Scale Output. For the calibrator, that output is 10 bar, while for the pressure transducers that is 17bar/100mV.

tainty of the measurements as $f_{P_j} = \pm 0.001458\%$. Again, this was found using the t -distribution, as for the regression analysis.

Physical properties: The way the transducer are mounted on the pipe give rise to uncertainties with respect to the actual pipe-diameter. Since the values of interest are located at the centerline of the system, the distance from the sensing element to the pipe-center is a source of uncertainty. Incorporated in this distance is whether or not the transducer actually was mounted flush with the internal pipe-wall. The pipe used in the experimental rig have a diameter tolerance of $e_R = \pm 0.1\text{mm}$. The pipe-radius was, $R = 50\text{mm}$, and it was decided to add $e_{flush} = \pm 0.2\text{mm}$ to account for the flush-mounting. The uncertainty associated with the calculation of the hydrostatic pressure at the pipe-center then becomes

$$e_{P_i} = e_R + e_{flush} = (\pm 0.1 \pm 0.2)\text{mm} \quad (3.3)$$

and the relative uncertainty becomes

$$f_{P_i} = \frac{1}{R} \left[(e_R)^2 + (e_{flush})^2 \right]^{1/2} = 4.4721e^{-3}\% \quad (3.4)$$

and can be seen as another systematic uncertainty in the pressure measurements.

Finally, using the RSS-method, the total uncertainty of the pressure measurements are

$$f_{P_{tot}} = \left[(f_{P_{cal}})^2 + (f_{P_h})^2 + (f_{P_j})^2 + (f_{P_i})^2 \right]^{1/2} = 0.11277\% \quad (3.5)$$

The dominating factor of the total pressure measurement uncertainty can be seen to be the systematic uncertainty of the transducer itself. Given that the FSO-error is dependent on most of the relevant systematic factors, which makes it relatively large compared to the rest, it's dominance was to be expected.

3.2.3 Uncertainty in strain measurements

The output from the strain gages are read directly during the measurement. In addition, due to availability of the right equipment, the gages was not calibrated before installation on the rig. Since the output was to be used to observe relative change, this was not seen as problematic. From the measurement process, five sources of error can be found; errors from installation, e_{sm} , the gages transverse sensitivity, e_{st} , temperature change, e_{sT} , the bridge's nonlinearity, e_{sn} and the random uncertainty of the strain gage, e_{sr} .

Misalignment: The strain gages are mounted axially, so that they react to the elongation and contraction of the pipe-wall. Any deviation from the axial centerline of the pipe will result in a in mounting angle, $\theta = \gamma \pm \beta$, where θ , γ and β are the actual, intended

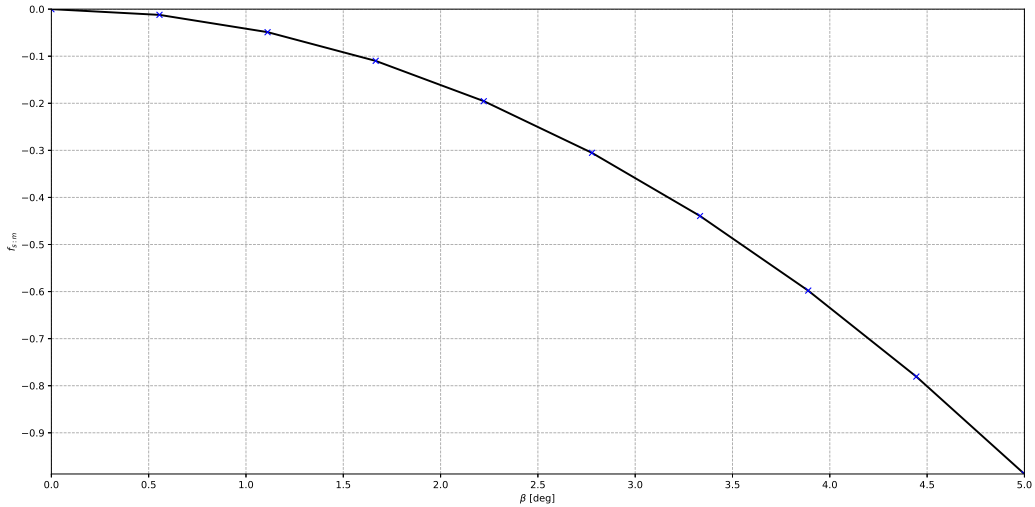


Figure 3.2.1: Misalignment uncertainty, f_{sm} , plotted against misaligned angle, β .

and misalignment angle, respectively. The assumed/measured deviation from intended mounting angle is found to be $\beta = 2^\circ$. Using equation (B.4), this gives a uncertainty from misalignment as $f_{sm} = -0.15834\%$. A visualization of this, with $\beta \in (0, 5)$ is shown in figure 3.2.1. It highlights the importance of accurate installation of the gage, because small deviations from intended angle quickly adds uncertainty to the measurements.

Transverse sensitivity: This error arise from the specimen's transverse contraction to longitudinal elongation⁴. The transverse sensitivity of the gages used here are given in documentation as $K_t = -0.1\%$. These errors proved harder to quantify correctly, mainly due to the fact that no strain measurements where taken in the circumferential direction. Using equation (B.5) and the stress-strain-relation for plane stress (see equation (B.6) the error because of the transverse sensitivity as $f_{st} = 2.27\%$. This must be seen as a very conservative estimate, when both stresses (σ_z , σ_ϕ) are approximations as well, using equation (2.6) and (2.5). Nevertheless, the type of strain gages that where used for the measurements, metallic foil gages, are said to be more sensitive to transverse influence due to the relatively large area of the resistive grid-lines [22].

Temperature: These errors will come from the change in gage resistance when the operating temperature changes. Steps where taken during the measurement to allow the pipe-wall and strain gage to be cooled down by the flowing water to ensure steady conditions during the measurements. For that reason, the uncertainties associated with temperature are neglected. Some details to the sources are given in appendix B.1.2.

⁴ See section 2.1.2

Nonlinearity: These errors originate from the fact that the bridge become unbalanced as the resistance in the gage changes. When the strains measured are assumed small, as they are for most metals, the nonlinearity error are usually small and there neglected. For the experiments described here, the nonlinearity uncertainty was calculated to $f_{s_n} = 0.005816\%$, using equation (B.8). Compared to the two other uncertainty-factors considered, this will not influence the total significantly, but will be included for completeness.

Strain gage: The random uncertainty for the strain gage output was estimated from a collection of steady state measurements to be $f_{s_r} = \pm 0.000388\%$. This was done in the same fashion as for the pressure transducer, using the t-distribution.

The total uncertainty of the strain measurements can then be calculated to

$$f_{s_{tot}} = \left[(f_{s_m})^2 + (f_{s_t})^2 + (f_{s_n})^2 + (f_{s_r})^2 \right]^{1/2} = 2.2755\% \quad (3.6)$$

The uncertainty for the strain measurements are clearly heavily influenced by the transverse sensitivity error of the measurements. This is consistent with what is found in literature, given the type of gage used. It should be noted that using multi-axis gages, so-called rosettes, would make the actual strains in the transverse direction available from measurements. With this, more accurate estimates of the dominate uncertainty could be obtained. It is also believed that the uncertainty could be lowered by choosing a different type of gage, where several other, similar types exist, based on other resistive materials.

3.2.4 Transient repeatability

For the validation process, it is the dynamic measurements during the waterhammer which are of interest. The pressure transducers were calibrated using their stationary response to a given pressure, and the uncertainties given above for both the measurands were, for the most part, estimated using the steady state response. Little is then known of the dynamic behavior of the instruments. Repeated measurements series, using the same initial conditions, were therefore conducted to check the repeatability in the dynamic region. This was harder to quantify, but comparison plots for both measurand for the different initial conditions can be used to visualize if the instruments behave similarly when exposed to similar conditions.

NUMERICAL MODELING

All numerical studies of physical systems will demand some sort of modeling. How the model performs compared to its real-life counterpart depends on the assumptions and simplifications necessary, as well as the complexity of the different system parameters. The trade-off of what to include and disregard has to be decided on the basis on what one wishes to gain from the resulting predictions. The system under consideration, the extended waterhammer equations, has been modeled using the method of characteristics (MOC) and the development of the model mainly follows the approach and notation found in [4]. The main assumptions and simplifications, together with some of the major consequences of using MOC, will be addressed here. Essential themes will therefore be the problem mesh, boundary conditions and pipe-wall friction.

4.1 Simplifications and Assumptions

The mathematical basis for the extended waterhammer equations, or four-equation model, is the two-dimensional Navier-Stokes equations and the two dimensional momentum equations for the fluid and surrounding pipe, respectively. The resulting model is valid for slender, straight, thin-walled pipe with a circular cross-section. The material, as well as the fluid, is assumed homogeneous, isotropic and linearly elastic, only subjected to small deformations. Considering only long wavelengths in the system, together with the assumption of axial symmetry, makes the final mathematical model one-dimensional, with variables depending only on the z - and t -axis. This also allows the wave propagation velocities to be considered constant [4].

A consequence of the one-dimensional assumption is that all predicted values are averaged over the respective cross-sectional areas. For the fluid this is the inner pipe area, while

the structural values are averaged over the pipe-wall area. This means that all predictions are considered constant over the cross-sections.

Another restriction which is originally put on the model is that the structure has to be thin-walled, meaning that $r/e \gg 1$. The reason this needs to be fulfilled, is because it allow the hoop stress, σ_ϕ to be assumed uniform across the pipe-wall and the radial stress, σ_r , to be neglected. These assumptions are necessary to arrive at the one-dimensional four-equation model. Nevertheless, investigation on the MOC-model used here where the effect of accounting for thickness have been done in [23] and the results presented further validates the one-dimensional assumption for a $r/e \rightarrow 2$.

4.2 Domain Discretization and Physical Constant Modification

The computational grid used in the computer program to solve the four-equation model is shown in figure 4.2.1. The lines emerging from points, A_i are called the system's characteristics, and are paths along which the solution travel. They arise from the transformation of the mathematical model using the MOC and their slopes are defined by the system eigenvalues¹. The four equation model has four distinct and real such roots found as

$$\lambda_i = \pm \left(\left[\frac{1}{2}q^2 \mp (q^4 - 4(c_f c_s)^2) \right]^{1/2} \right)^{1/2} \quad (4.1)$$

where q is a collection of terms

$$q^2 = c_f^2 + c_s^2 + 2\frac{\nu^2 R}{Ee}(c_f c_s)^2 \quad (4.2)$$

and the solutions to λ_i will be defined as

$$\lambda_i = \begin{cases} \pm \tilde{c}_f & \text{for } i = 1, 2 \\ \pm \tilde{c}_s & \text{for } i = 3, 4 \end{cases} \quad (4.3)$$

As seen from equation (4.2), the system eigenvalues depend on the theoretical wave propagation velocities, as well as a factor controlled by the Poisson's ratio, ν and other physical parameters. The \tilde{c}_j can be seen as the FSI-wave velocities for a specific setup. Consequently, ignoring the Poisson coupling, will give $\tilde{c}_i = c_i$.

Solving the system can be done by following the four characteristic lines from points where the solution is known, A_i , to a common point of intersection, Q . Numerically this was done by choosing constant increments in the spatial and temporal direction, say Δz and Δt , then using a marching algorithm to iterate forward in time. Due to differences

¹ The eigenvalues are found solving the system's characteristic equation, $|\mathbf{B} - \lambda\mathbf{A}| = 0$. Specifics about this can be found in [4, 24]

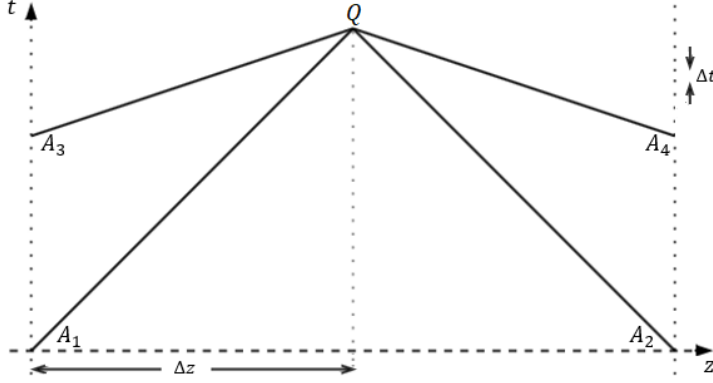


Figure 4.2.1: Four-equation model's characteristic lines in the stress-wave grid configuration (Adaption from [4]).

in eigenvalue-pairs, $\lambda_{1,2}$ and $\lambda_{3,4}$, the corresponding line-pairs will have different slopes. These slopes can be defined as

$$\frac{\Delta z}{\Delta t} = \lambda_i \quad (4.4)$$

The chosen grid has $i = 3$, making it a so-called stress-wave grid, which accounts for the differences in slopes by picking $\Delta t \ll \Delta z$, allowing lines to emerge from points further back in time. There exist several other grid-configurations that can be used to solve the same model, but the configuration in figure 4.2.1 eliminates the need for interpolation to solve the system at it's boundaries. This is seen as advantageous because interpolations tend to give rise to numerical damping [4].

How much smaller the temporal increment must be chosen than the spatial to ensure that characteristic actually emerge from a grid-point can be determined by using

$$\frac{\tilde{c}_s}{\tilde{c}_f} \approx \frac{b}{a} \quad (4.5)$$

where b, a define how far the characteristics must reach back to find an initial state. Given that grid-points must be treated as integers, demands the ratio, b/a , to be rational. For the experimental setup these values become

$$\frac{\tilde{c}_s}{\tilde{c}_f} = 4.41958 \approx \frac{22}{5} = \frac{b}{a}$$

The rational number demand forces a slight adjustment of the eigenvalues by modification of the physical properties they depend on. Adjusting the mass densities using the characteristic equation (see equation (4.2)) is suggested by [25] as a way to minimize the

introduced error due to the changing of eigenvalues, because it is possible to choose the ratio sufficiently close to the actual \tilde{c}_s/\tilde{c}_f . Doing this, the changed mass densities will fall within measurement accuracy range [4].

4.3 Boundary Conditions

It was observed from simulation done during the project work that altering the boundary conditions will significantly change the entire system response. It is therefore seen as an important factor to model as close to real as possible. Two additions have been done to the downstream boundary as a result of those observations, namely incorporating a valve-closure time and modeling the system's terminal point using a mass-spring-damper approach.

4.3.1 Mass-spring-damper-model

In order to make the model more physically accurate, some work has been done to the downstream boundary model, giving two new additions. During the project work, two types of boundary conditions were tested, one where the valve is kept rigidly fixed and one version allowing axial motion (free valve). According to the definition of the junction coupling (see section 2.1.2), a fully restrained terminal point will in reality mean neglecting this mechanism. For a real-life experiment, some motion must always be assumed. Formerly, the free valve-condition have only depended on the acceleration of the end-point. To make it even more accurate, a mass-spring-damper-model can be used to account for the pipe material's damping and elasticity as well.

The model proposed for a free valve-condition is depicted in figure 4.3.1. Evaluation of that FBD yields

$$A_{fp} - A_s \sigma_z = \pm m \ddot{u}_z \pm c \dot{u}_z \pm k u_z \quad (4.6)$$

where A_i is the respective areas where the forces act, m is the valve's mass and c and k are the damping and spring-stiffness coefficients. Estimation of c can be done using a relation from a simple oscillator, namely

$$c = 2\xi\sqrt{kM} \quad (4.7)$$

where ξ is the damping ratio and M is the pipe's and valve's masses combined. The damping ratio is usually assumed $\xi < 1$ for underdamped systems. For finding k , one can use

$$\omega_n = \sqrt{\frac{k}{m}} \Rightarrow k = m\omega_n^2 \quad (4.8)$$



Figure 4.3.1: Free-body-diagram of a unrestrained, closed valve. The pressure force acts over an area A_f and the resulting axial stress acts over a area A_s [4].

where ω_n is the systems undamped natural frequency, which can be estimated with

$$\omega_n = \frac{1}{4L} \left[\frac{E}{\rho_s} \right]^{1/2} \quad (4.9)$$

The expression is valid for a empty pipe modeled as a cantilever beam with a fixed and free end, subjected to axial oscillations. This must only be seen as a crude approximation, because considering a fluid-filled pipe will influence the natural frequency [26].

4.3.2 Non-instantaneous valve closure

Finding a model which describes the flow through the valve as a function of opening can be done using an orifice equation. This is a relationship between the fluid discharge, Q , and pressure, P . A common way to represent this is

$$Q_z = C_d A_v \sqrt{\frac{2\Delta P_z}{\rho_f}} \quad (4.10)$$

where C_d and A_v are the valve discharge coefficient and area of valve opening, respectively. The steady equivalent can be expressed using $(C_d A_v)_0$, $(Q_z)_0$ and $(P_z)_0$ instead [6]. Considering a similar relationship, now taking the FSI-effects in to account as well, defining Q_{rel} as

$$Q_{rel} = \frac{V_{rel}}{A_v} = \frac{V_z - \dot{u}_z}{A_v} \quad (4.11)$$

the equation (4.10) can be written as

$$(V_z - \dot{u}_z) = C_d \sqrt{\frac{2\Delta P_z}{\rho_f}} \quad (4.12)$$

Expressing the flow through the valve relative to the steady state conditions can then be

Table 4.1: Chosen variables to adjust the valve closure-equation to the experimental case.

Variable	Value	Variable	Value
x_i	1.0	x_1	0.4
t_c	0.125	E_i	[2.0, 3.1]
t_p	$0.5 t_c$	t_{c1}	$0.646 t_c$

done as

$$\frac{(V_z - \dot{u}_z)}{(V_z - \dot{u}_z)_0} = \pm \tau(t) \left[\frac{|\Delta P_z|}{|\Delta P_z|_0} \right]^{1/2} \quad (4.13)$$

where ΔP_z is the pressure-loss across the valve. This orifice equations was proposed in [4], and introduces a nonlinear boundary condition when valve closure-time is taken into account. The nonlinearity complicates the process of implementing it in the existing code.

In the above expressions, the τ has replaced the relative discharge coefficient, $C_d/(C_d)_0$. This a dimensionless closure-function which is given by the specific valve-characteristics and shall control the amount of kinetic energy which is lost due to the escaping fluid during the transient. For the valve-configuration used during the experiments, a two-speed closure process is proposed by [27]. This is to better capture the characteristic. A variation of this two-speed model was obtain for the experimental case and is given as

$$\tau(t) = \begin{cases} v_i \left[1 - \left(\frac{t}{t_{c1}} \right)^{E_1} \right] & \text{for } t < t_p \\ v_1 \left[1 - \left(\frac{t - t_p}{t_c - t_p} \right)^{E_2} \right] & \text{for } t_p \leq t \leq t_c \\ 0 & \text{for } t > t_c \end{cases} \quad (4.14)$$

where v_i and v_1 are the initial and second stage relative nozzle opening, t_{c1} and t_c the first stage and total closing time, t_p the second stage start time and E_i case-specific empirical coefficients. To adjust the above equation to the experimental case, the values for the variables were chosen as given in table 4.1, giving the characteristic shown in figure 4.3.2.

To omit the nonlinearity in equation (4.13) a linear relationship can be used. One proposed by [26] was seen as a more suitable choice, because it simplifies the orifice equation by neglecting the pressure-term on the RHS. Consequently, the relative velocity is assumed to only depend on the dimensionless valve closure, τ . Doing this, equation (4.13) becomes

$$\frac{(V_z - \dot{u}_z)}{(V_z - \dot{u}_z)_0} = \pm \tau(t) \quad (4.15)$$

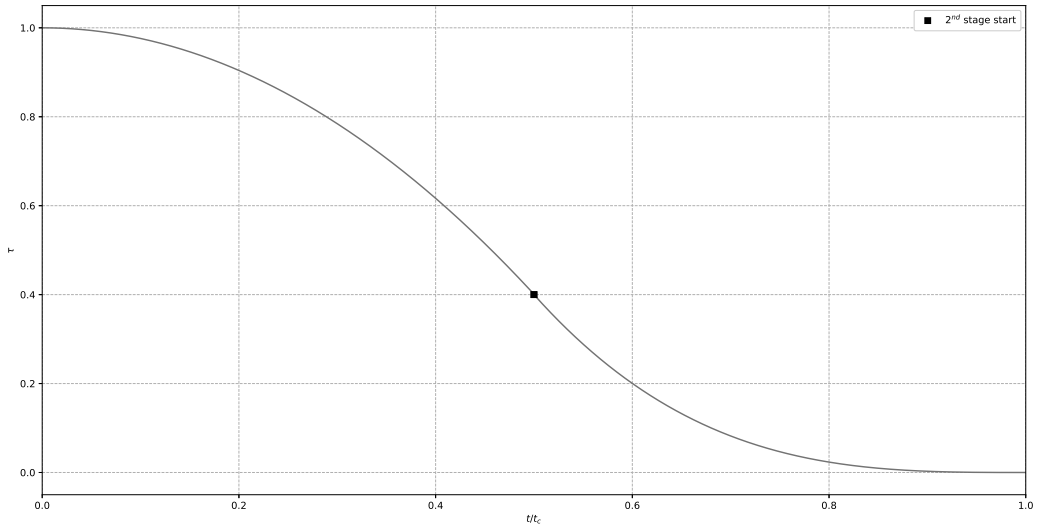


Figure 4.3.2: Valve closure characteristic with the values from table 4.1, plotted against dimensionless time, t/t_c

Solving for V_z yields

$$V_z = \dot{u}_z \pm (V_z - \dot{u}_z)_0 \tau(t) \quad (4.16)$$

This expresses the fluid velocity at the boundary as a linear function in time, depending on the axial pipe-end motion and valve opening [26].

4.3.3 Challenges concerning new boundary conditions

Implementing new and more complex boundary conditions in the numerical model did not prove as trivial as first expected. Introducing non-instantaneous valve closure to the simplified massless, free valve condition proved stable and was able to model the dissipating energy associated with the escaping water to some degree. When the mass-spring-damper-model was added to the free-valve condition, the response tended to become very unstable, resonating out of proportions if the simulation time is increased.

This was especially evident with choosing a close-to-accurate valve mass and estimating the spring stiffness and damping coefficients with the expressions in section 4.3.1. Numerical resonance was observed occurring in front of steep gradients in the solution. If allowed to accumulate over time, such ripples will make the calculations highly unstable. Even putting the mass and coefficients to unity could not completely remove the instability. Evidently, there exist something in the implementation or formulation of the boundary condition that creates this. For that reason, the mass-spring-damper-model will not be included as a part of the results.

CHAPTER 5

RESULTS

A large part of the work done during this thesis has revolved around the experimental setup, instrumentation, and the measurements done on the waterhammer-rig. The specifics about the experiments were described in chapter 3. Combined with some alterations to the code, the experiments were conducted in an effort to validate and verify the simulations done with extended waterhammer equations. To highlight some of the features where the calculations and measurements match and mismatch, the experimental and simulated data will be compared and commented on. Emphasis will also be put on showing the repeatability and the presence of fluid-structure interaction effects in the pressure and strain measurements.

All measurement data presented here was taken at a sampling rate of 25kHz. For the most part, all time-series that will be shown from the onset of the transient and 0.5 seconds ahead in time. This is where most of the interesting physics are happening, and also where the model and measurement data was assumed to be most equivalent. It should be noted that the accelerometer used on the rig were found to be broken during post-processing, which made data obtained with it unusable.

5.1 Experimental Results

The following section will show the pressure-time and strain-time plots of a selection of the experimental data obtained from the rig. An effort will be done to show the repeatability and reproducibility in the sensors and experiment during the transients, as well as showing the typical dynamic behavior that was observed during the experiments. Comparison will also be done between measurement series done on the rig with the nozzle bolted to the

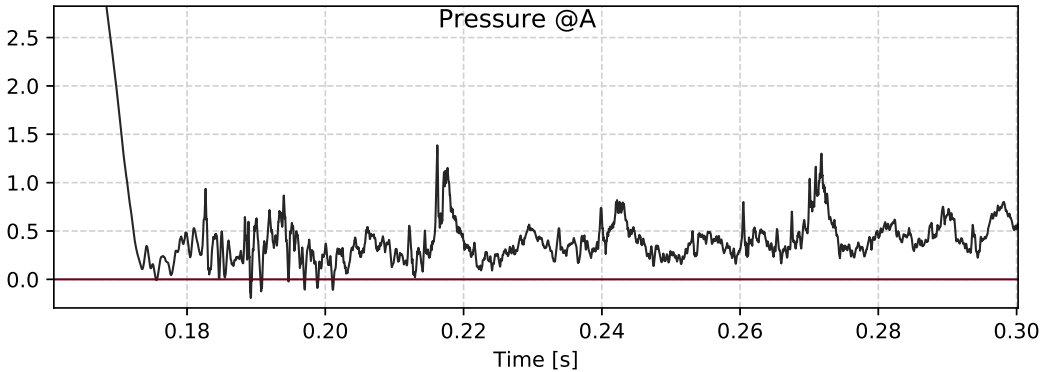


Figure 5.1.1: Typical behavior obtained at measurement-point A. Assumed to be brought on by entrapped air in the nozzle

downstream discharge chamber, and when it was allowed free motion. With this, different boundary conditions can be investigated.

The time-series in figure 5.1.1 shows a close-up of the typical recorded response at measurement-point A, which is the one closest to the downstream nozzle. Compared to the behavior at the three other points, the behavior was somewhat unexpected. More so, the simultaneous response captured by the strain gage (see figure 5.1.3, top two plots), show a more expected response. Typically, this is the point on the rig where the calculations predict the highest amplitudes and the most violent motion. But the recorded pressure fluctuations shows signs of being completely damped out as soon as the reflected wave returns. The effect was also found to be systematic and can be observed for all data-series recorded at measurement-point A. Several factors can be the reason for this, one being that entrapped air exists inside the nozzle, another that the sensor have become damaged. Since the occurrence are found to be systematic,

Figures 5.1.2 and 5.1.3 are showing the behavior of the transducers and gages recorded at identical initial and setup conditions. They consist of two pairs of measurements taken at the same point about 15 minutes apart. It can be seen from the plots that the instruments tend to capture the amplitude of the peaks from series to series. A slight shift in phase has been observed to change between the measurements-series. The effects are not that apparent in the series in figure 5.1.2, since they were obtained with only minutes between, but the shift is more observable if measurements were taken further apart¹. Nevertheless, both the pressure transducers and strain gages are believed to exhibit satisfactory repeatability during the transient. The experiment is also showing reproducibility across different series and from day to day.

Another phenomenon typical for the rig that should be commented on, is the behavior shown at measurement point B in figure 5.1.2. The first and second reflected waves usually resulted in pressures down to $P = 0$ bar, presumably creating a vapor cavity that dissipates

¹ Comparison plots can be found in figure A.1, showing a slight change of phase in the fluctuations, with the exception of the first and second peak.

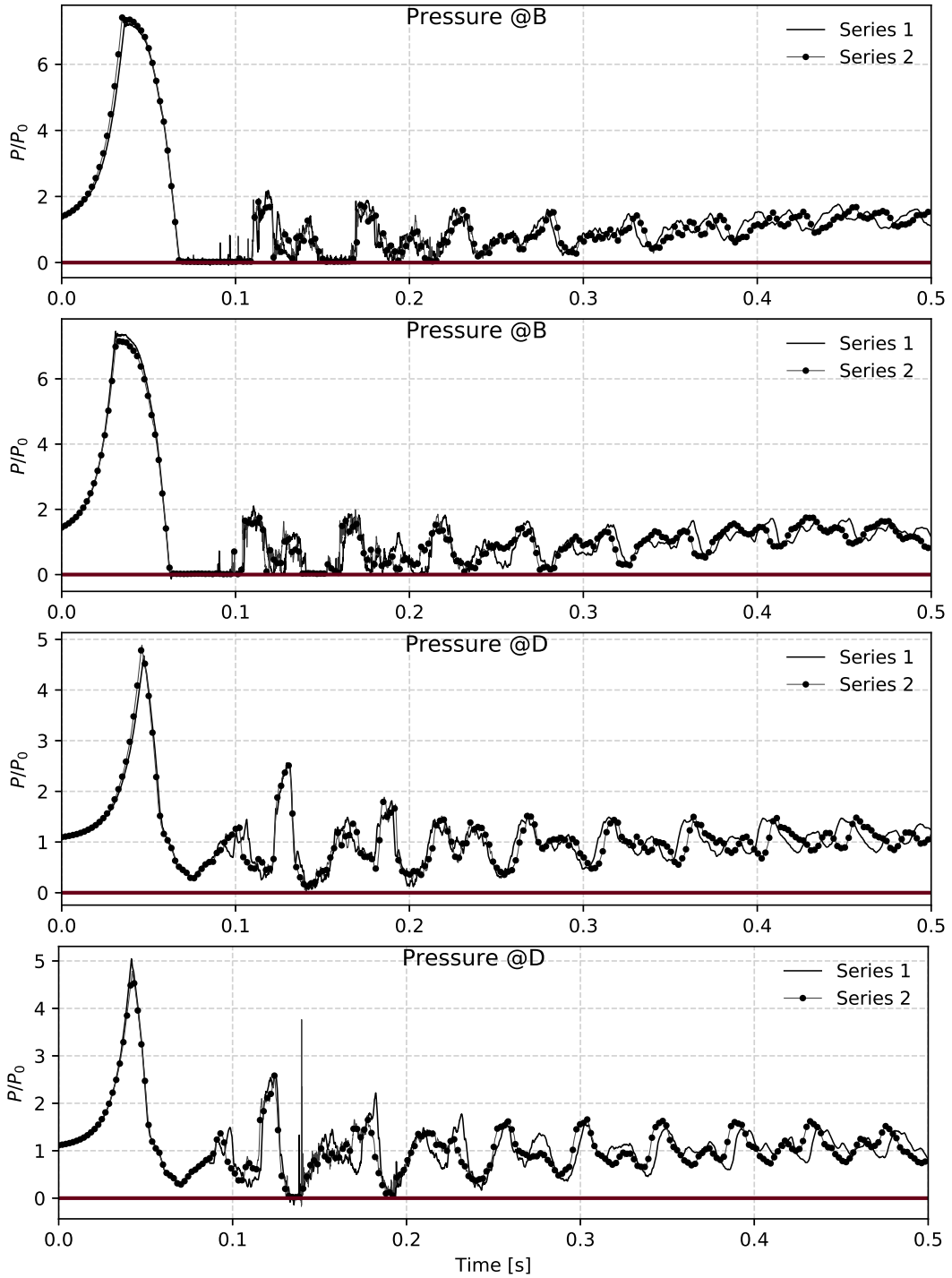


Figure 5.1.2: Pressure-time behavior of the pressure transducers at $V_0 = 0.980$ m/s. Showing first 0.5 s of the transient. Red line indicates $P = 0$ bar. Series 1 and 2 are obtained only minutes apart.

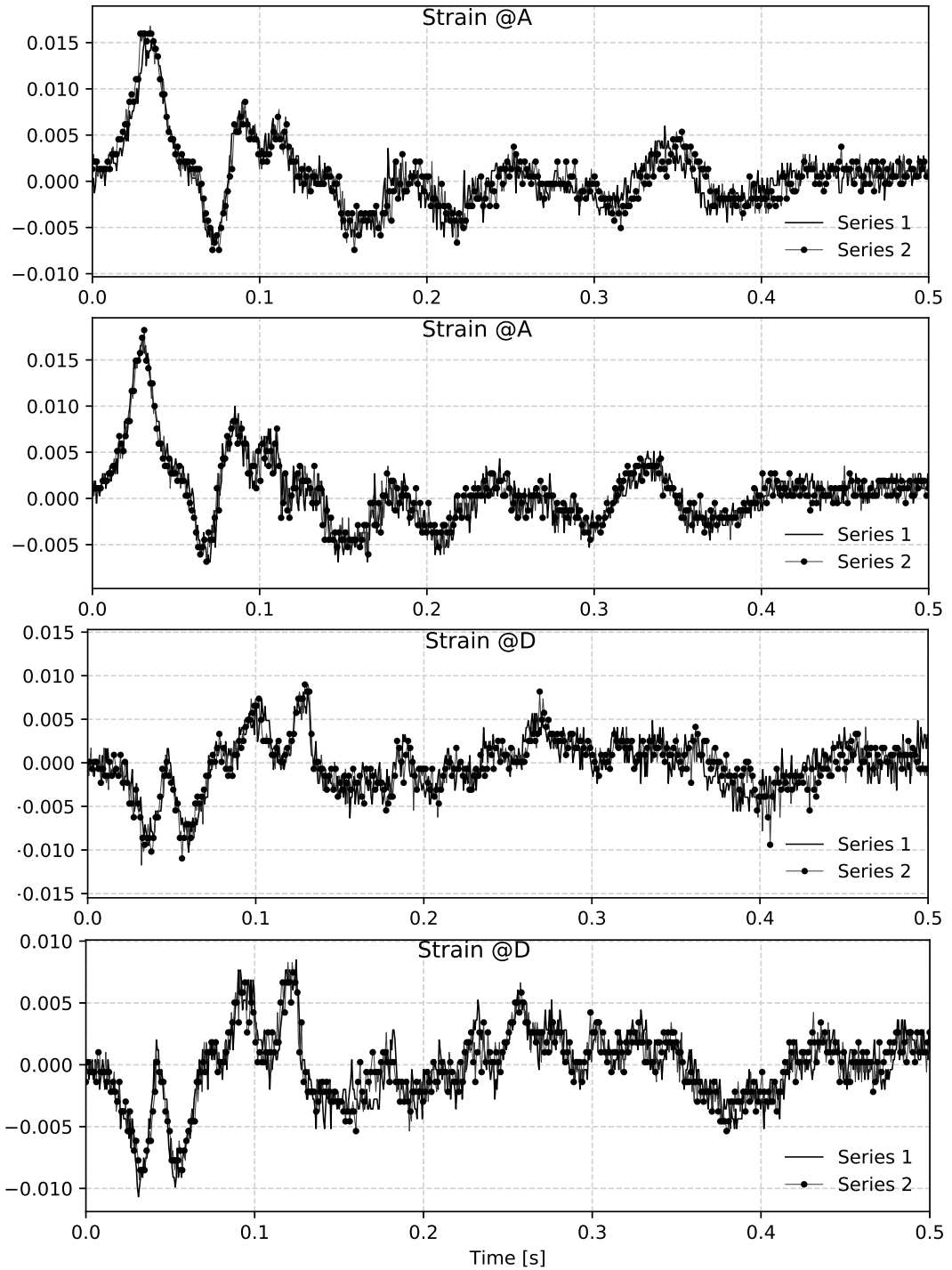


Figure 5.1.3: Strain-time behavior of the strain gages at $V_0 = 0.980$ m/s. Normalized for $\varepsilon_{z,0}$ and showing the first 0.5 s of the transient. Red line indicates the relative centerline. Series 1 and 2 are obtained only minutes apart.

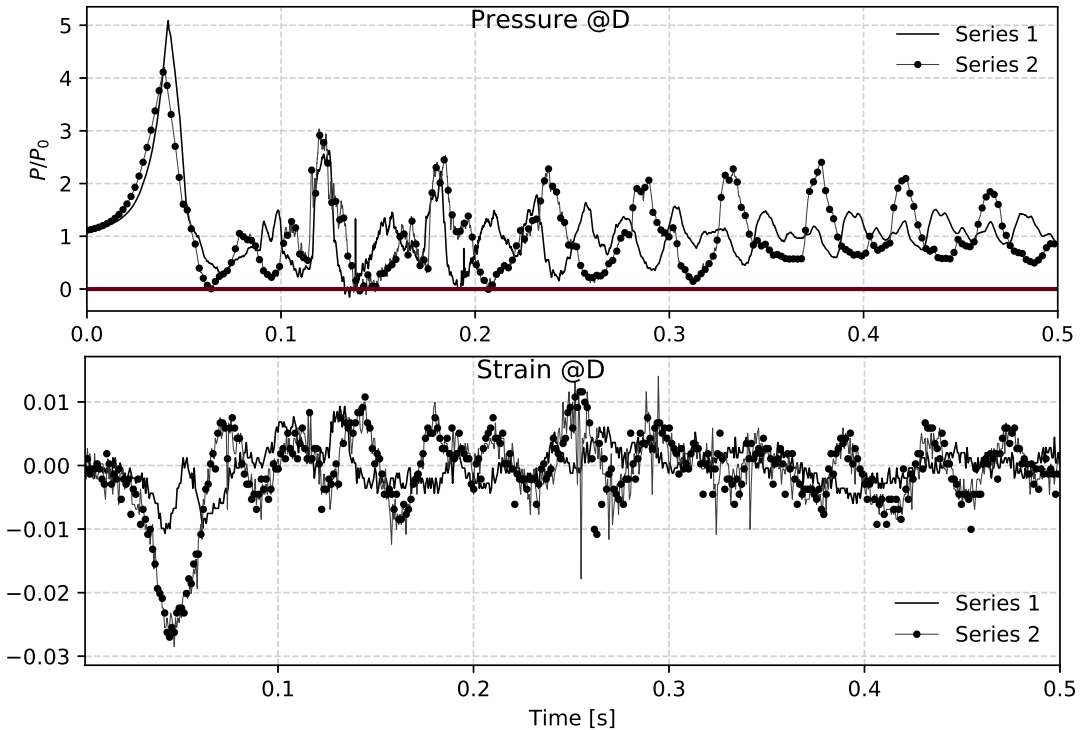


Figure 5.1.4: Comparison of boundary conditions for the experimental rig at measurement-point D. $V_0 = 0.980$ m/s.

the energy in the waves. It can be noted that the same behavior was observed for most of the time-series extracted from points B and C. This behavior was not a regular problem for point D, although it can be seen here to come fairly close.

A suspected FSI-effect which should be present in the measurements is the precursor wave and is found as a small disturbance which subtracts or adds to the global pressure response. Such perturbations can be seen in the presented pressure-time-plots, and were especially evident on the crests of the fluctuations. These effects can also be observed to die out as the energy in the system dissipates over time and are usually spent after about 0.3 s.

The differences between the bolted and free valve should also be commented on. Figure 5.1.4 show the recorded strain and pressure response for the cases where the valve was bolted to (series 1) and detached from (series 2) the discharge chamber. The change of boundary conditions affect the response by giving longer lasting fluctuations and higher amplitudes, especially the for the measured strain. A much greater shift in phase can also be observed for both measurands. The most remote end of the pipe is chosen to show this, because the closing mechanism and operator influence with the rig are believed to have a lesser impact here².

² See description of operating procedure in section 3.1.3

Table 5.1: Model and experimental input-values for the simulation setup

Physical properties					
L	24.2	Pipe length [m]	r	0.05	Pipe radius [m]
e	0.002	Pipe thickness [m]	ν	0.3	Poisson's ratio
ρ_f	1000.0	Mass density [kg/m ³]	ρ_s	7700.0	Mass density [kg/m ³]
E	200.0	Young's modulus [GPa]	K	2.1	Elastic modulus [GPa]
t_{c1}	$0.6t_c$	1 st stage closing time	E_i	[1.0, 1.0]	Empirical coefficients
Iteration constants					
b/a	22/5	Wave speed adjustment	t_{max}	0.5	Transient duration [s]
Δt	4.0 e^{-5}	Temporal step size [s]	m	12500	Nodes in time
Δz	1.21	Spatial step size [m]	n	21	Nodes in space
Steady state conditions, for $t < 0$					
P_0	-	See table 3.3	V_0	-	See table 3.3
σ_z	-	0.0	ε_z	0.0	Relative strain
$\dot{u}_{z,0}$	0.0	Axial velocity [m/s]	u_z	0.0	Axial displacement [m]

5.2 Simulated and Experimental Response

In order to validate the numerical calculations of a waterhammer-event, experimental data-series were plotted against equivalent data-series produced by the straight-pipe, extended waterhammer equation-code. The additions presented in chapter 4 were implemented in the code to increase the similarities between the two cases. Furthermore, the numerical input-values for the simulations are given in table 5.1. Running the computer program with these as input, the calculated output was obtained as shown in figure 5.2.1. It is important to note that the variables for the valve-closure characteristics proposed in table 4.1 were changed due to the fact that the calculations became unstable with that setup. The changes can be found together with the other input-values.

A sample of plots showing a comparison the calculated and measured pressure response of the system can be found in figure 5.2.2. Firstly, the calculation struggle to estimate the first pressure peak when the nozzle is allowed to a realistic closure time. For the following reflected wave, the predictions are more accurate, but one can already here see that the wave propagation velocities are beginning to deviate between the calculations and the measurement data. The low-pressure zones are also overestimated by the computer program. The comparison for point C is given to highlight the effects from a forming vapor cavity in the pipe. Some equality can nevertheless be found, the period between the first and second peak is in fact predicted correctly, showing that the propagation velocities can be assumed similar during the first few moments of the transient.

The measured and calculated strain response is shown in figure 5.2.3. As for the pressure-time-behavior, much of the same effects are present here as well. Especially evident is the significant strain-peaks that is recorded in the first moments of the exper-

5.2 Simulated and Experimental Response

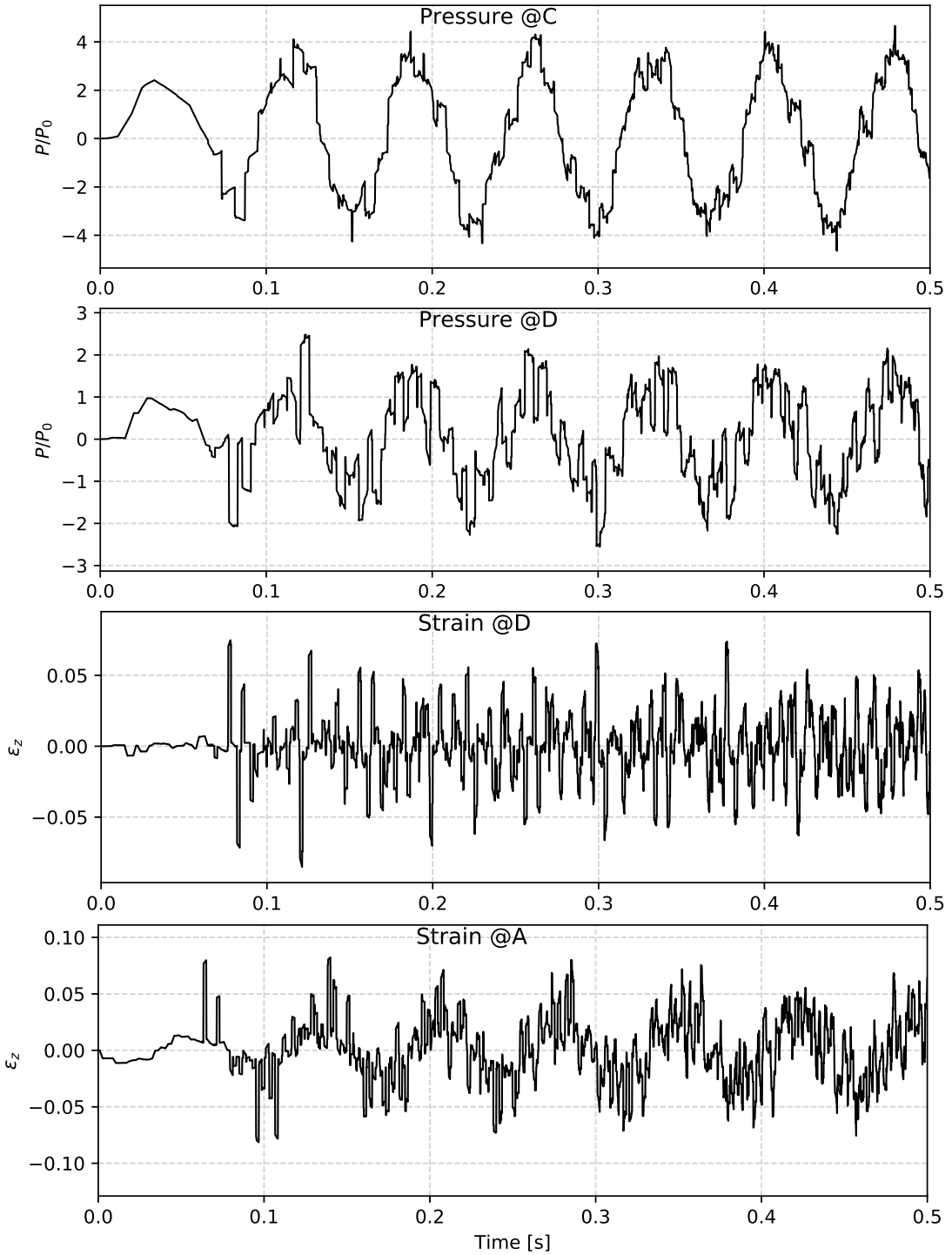


Figure 5.2.1: Showing calculated response of the experimental setup for $V_0 = 0.980$ m/s, with a free, massless valve, $t_c = 0.125$ s.

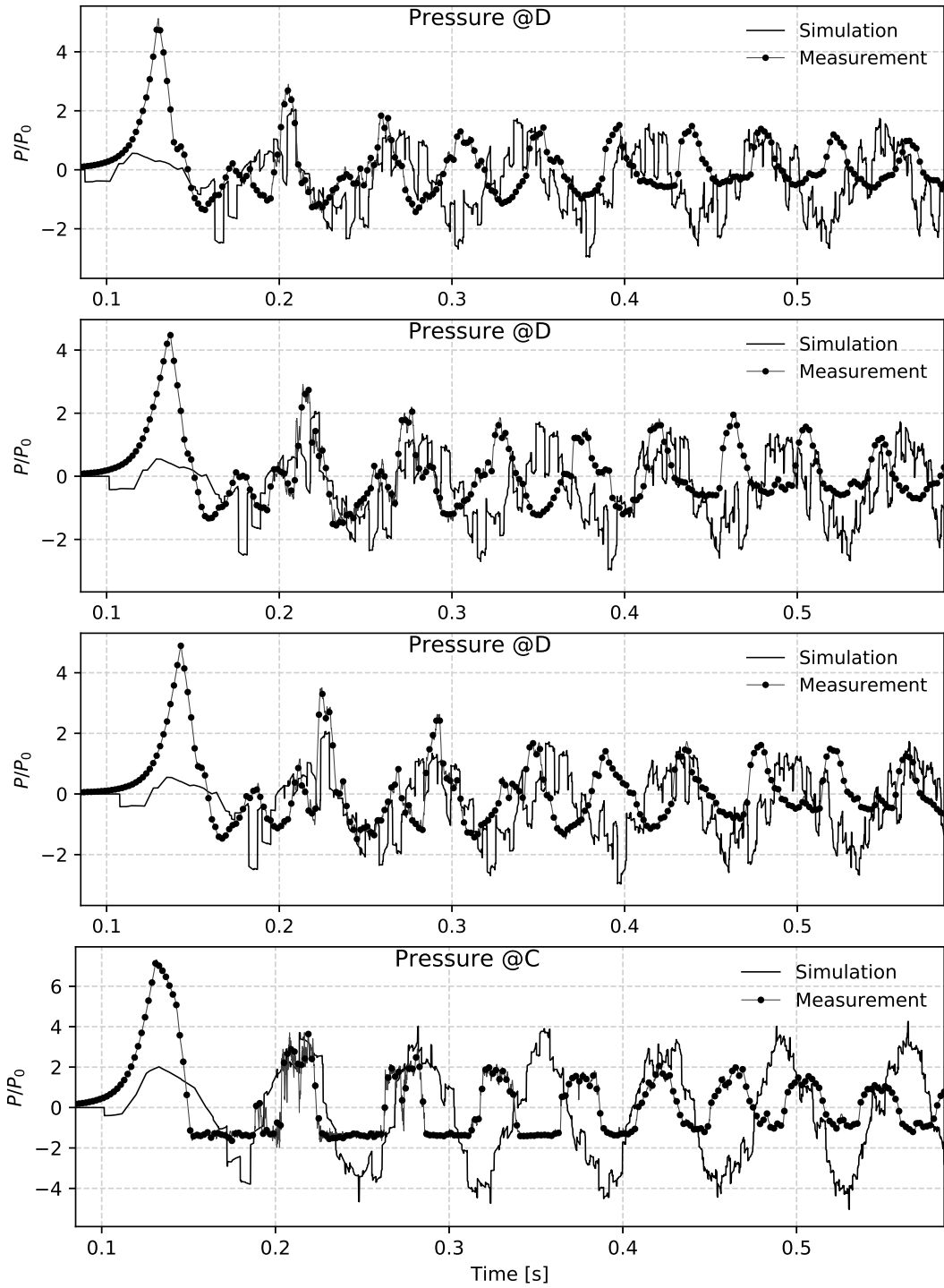


Figure 5.2.2: Measured pressure vs. simulated at a flow velocity of $V_0 = 0.980$ m/s. Valve detached from discharge chamber.

5.2 Simulated and Experimental Response

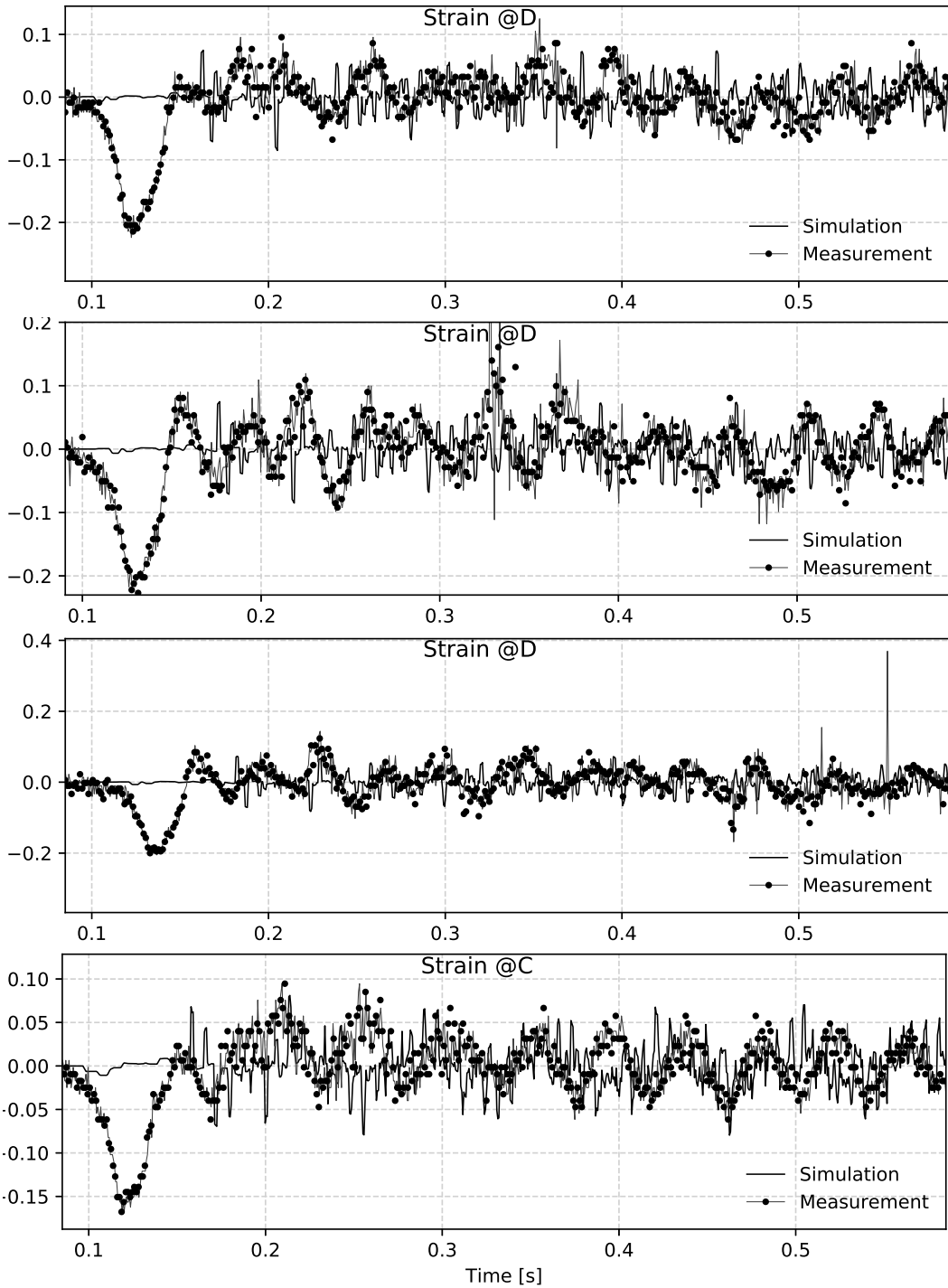


Figure 5.2.3: Measured strain vs. simulated at a flow velocity of $V_0 = 0.980$ m/s. Valve detached from discharge chamber.

iment. Both the calculations and measurements exhibit notably more rapid fluctuations compared to the pressure data. This is to be expected, due to the differences in wave propagation velocities. Continuing with the comparison, the estimated response struggle to follow the general behavior that is recorded by the strain gages. The reason for this is thought to be that the general behavior of the recorded strain show a tendency to follow global fluctuations, resembling the pressure measurements.

5.2.1 Calculated variables

An example of the estimated response for the axial stresses, σ_z , can be found in figure 5.2.4 and is calculated from the strain and pressure measurements using equation (2.6). The first and second wave prediction at measurement-point B is fairly accurate, especially with respect to timing. The same deviation in wave propagation velocity can also be observed here, which is natural, considering that the response depend on the shape and magnitude of the recorded strain and pressure. As for calculation of the axial displacement velocity, all results obtained with proposed strain-displacement-relation in equation (2.10) proved the calculations inaccurate. One can see this in figure A.5, where the predictions to \dot{u}_z are overestimated by a factor of 10^2 . For all obtained results, these are the ones that deviate the most with respect to predicted magnitude. Although derived from known, mechanical

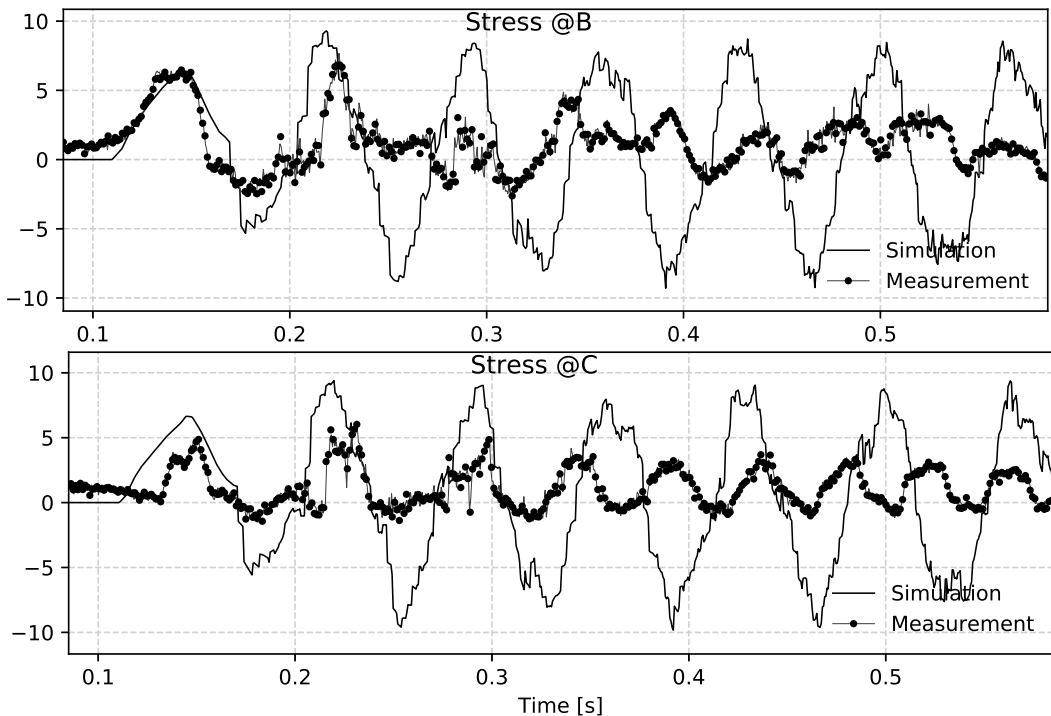


Figure 5.2.4: Showing a representative derived response compared to simulation for the axial stress, σ_z . $V_0 = 0.980$ m/s.

relationships they should only be taken as rough estimates for their actual responses. They are included in order to verify the expressions used in the predictions and because their values, in the opinion of the author, are more understandable than the relative values of strain.

CHAPTER 6

DISCUSSION

The validation and verification process will be based both on the comparison of results and the presence of fluid-structure interaction-effects in the measurement data. The following discussion will focus on identification of physical phenomena in the measurements, as well equalities and inequalities between the model and measured data.

6.1 Fluid-structure interaction effects

An important aspect of a verification process, was the identification of relevant physical phenomena in the measurements which verifies the mathematical assumptions and theories which the method and calculation are built on. Examples to such phenomena for the case studied here is the precursor wave (Poisson coupling), boundary effects (junction coupling) and the different wave propagation velocities in the system, those being the axial stress and pressure waves¹. The latter should be easily detected by a side-by-side comparison of the strain and pressure measurements at point D.

As stated in section 2.1.2, the axial stress waves can be influenced by anchoring-points and straight junctions, such as those present along the whole length of the pipe in the experimental rig. One should not expect that the structural waves are reflected purely from the valve and reservoir. The effect of this is that the reflection time of c_s may differ from the theoretical.

An interesting aspect to note, is that the strain measurements also show a tendency to follow the pressure peaks as well. This gives characteristic, global fluctuations in additions

¹ Theoretical description can found in section 2.1

to the structural ones. It is also suspected that these mask the weaker, faster response of the strain in the system.

The other significant FSI-effect in the system should be the junction coupling. The observed increase in amplitude and duration of the pressure and strain fluctuations when the terminal point was detached from the downstream restraint of the discharge chamber suggest that such effects exist. Releasing the nozzle also gave the system changes in the wave propagation velocity. The theoretical values of c_f (see equation (2.2)) finds it as dependent on the amount of restraint put on the fluid due to the surrounding structure. Allowing for increased axial motion² can therefore be seen as an easing of the axial restraint, consequently increasing c_f .

6.2 Model Validation

Considering the results presented in section 5.2, the main areas of interest in validating the numerical predictions will involve amplitude, frequency and energy dissipation. The model are able to predict the amplitudes of the positive pressure peaks, with the exception of the initial one, to a fairly satisfactory degree. The model clearly overestimates the negative amplitudes and the relative centerline differs. A reason for this can be that the experiments have been conducted at a fairly low steady state pressure, so the increasing magnitude of the pressure during the transient quickly made the troughs hit $P = 0$ bar, preventing further reduction. This is when a valve closure time, $t_c \neq 0$ are modeled. Similar predictions of the pressure and strain response are given in figure A.4 where the valve are closed instantaneously. Alternating the boundary condition clearly impacts the calculated response, and the predictions become more inaccurate.

The frequency of the pressure waves were found to deviate more between the data sets, and the measurements show that the wave propagation velocity was not constant over the course of the transient. This is a major prerequisite for the theoretical investigation of the waterhammer event. The frequency of the fluctuations are governed by the wave reflection time, which depend on the length of the pipe. If something blocks the fluid path, like a vapor cavity or entrapped air, the wave will feel a different length than the actual pipe-length. It could explain the increased frequency of the reflected waves, and is observable for most of the measurements-series obtained by the rig. Nevertheless, the frequency of first three reflected waves look to be prediction accurately.

The valve closure characteristics were implemented in the numerical calculations to model the energy-loss that happens if fluid is allowed to leave the system in the initial phase of the transient. The differences in predicted amplitude when this is allowed for and not, is very notable. The other source of energy dissipation that exist in the system is due to friction forces. Assuming steady shear stresses in the first moments of the transient can be partly verified by the observation similar positive pressures for the first 0.5 seconds,

² The nozzle must be assumed to experience some degree of movement even when rigidly bolted to the discharge chamber. This is due to the 0.99 meter of pipe between the nozzle and anchor-point (see figure 3.1.3d).

finding the energy dissipation negligible. The same can not be said with respect to the reduction of amplitude from the first and second peak or for prolonged calculations using the steady friction-assumption.

The model calculates the strain using the strain-displacement relation from equation (2.7) and the numerical derivation method of finite differences. Since the strain is the spatial derivative axial displacement, this provides a crude approximation, considering the relatively large time-step in the calculations ($\Delta z = 1.21$ m, see table 5.1). This is believed to be part of the reason for the lack of the global fluctuations that are observed in the measurement-data.

6.3 Model – Measurement Discrepancies

Several aspects differ between the presented numerical model and the experimental setup. The differences come from assumptions and simplifications done in order to arrive at the extended waterhammer equations, but also from the setup itself. Examples to such discrepancies are the friction and valve-closure model, and the presence of vapor cavities in the pipe during the transient.

6.3.1 Experimental setup

The laboratory setup has its limitations with respect to the phenomenon under investigation. Firstly, manually closing of the nozzle to initiate the transient introduces too much uncertainty in the time it takes the nozzle to become fully closed. Implementing a method for remote and automatic closure would certainly remove some of the uncertainty. Considering the calculated wave reflection time for the system, faster closure is also desirable, leaving more energy in the system.

The experimental setup also has its limitations due to the hydrostatic pressure in reservoir. Due to the way the rig was built a certain fluid velocity so water started flowing uniformly out of the nozzle at the downstream end. With only 0.55 m of physical water column in the reservoir, the steady state pressure was so low, it made the initial pressure change due to valve-closure sufficiently large so that the reflected pressure wave lowered the pressure down to $P = 0$, creating vapor cavities. Since the presence of such cavities are not considered in the numerical model, this is expected to be a major contributor to some of the discrepancies between the predictions and measurements. Larger cavities in the fluid will also influence the felt diameter of the pipe, as well as act as an energy sink, dissipating the initial potential energy in the system.

6.3.2 Numerical modeling

Several of the deviations between the model and the experimental setup are believed to be the sources of some of the differences seen between the two data sets. The most notable are the friction model and boundary-conditions, but some discrepancies can possibly be found with the characteristic mesh and wave propagation velocity that are used in the model.

Modeling the friction as steady throughout the calculations was expected to cause differences when compared to the realistic response. The specific factors which make this assumption inadequate to model the actual energy-loss due to friction are given in section 2.2.2, and are usually attributed to the fact that the fluid velocity profile is dependent on the r -component.

In an attempt to capture the effects of a more realistic downstream boundary, a mass-spring-damper-model was tried implemented in the calculations. The simulations experienced numerical instabilities when this was taken into account. Several modifications were done to mitigate the problem, but none were able to achieve this. More successful was the implementation of a valve-closure characteristic, which made the model able to account for some of the energy lost during the closure-time. Some difficulties were present here as well, due to the non-linearity in the original orifice-equation. Simplifying the equation proved more translatable to the existing method of defining boundary conditions in the numerical model. Whether or not the model was made more realistic is somewhat questionable, since some strange behaviors were observed for the first peak in the calculated data. This is almost completely removed, especially in the strain-calculations, in addition that a small negative step was created in the pressure-time-series (see figure 5.2.2 and 5.2.3).

Lastly, a note should be given to the mesh and theoretical FSI-wave propagation velocities. The spatial increment for the simulations were chosen on the basis of shortening the computation-time and still be able to obtain predictions for the corresponding measurement-points on the experimental rig. This made for a coarse grid and a small deviation in spatial position where the measurement data and calculated response were obtained from. Differences have also been found in measured and calculated system frequencies. The method of characteristics helps define compatibility equations which are considered constant between points on a path through the domain. To obtain the solution for a point in the domain, four such paths must intersect at that point. The FSI-wave propagation velocities are defined as the slopes of these paths. If they change over the course of the transient, these paths would change as slopes, and the the lines would not intersect at the desired grid-point. This may account for some deviations between the solution and measurement as well.

CHAPTER 7

CONCLUSION

The main objective of this thesis has been the verification and validation of a computer program describing the waterhammer-phenomena where fluid-structure interaction-effects are taken into consideration. This was to be achieved by conducting a laboratory experiment of a straight pipeline in a reservoir-pipe-valve-configuration. An additional goal have been the general study of fluid-structure interaction for hydraulic systems, to aid in a wider verification of the occurrence and relevance of the mechanisms of interaction that exist.

The validation of the computer program have been successful, but unfortunately only to a certain degree. The numerical model are able to predict the system amplitudes, at least for the positive peaks, at the measurement-point farthest upstream. The presence of vapor cavities in the vicinity of the other points has deemed the results more inconclusive. The FSI-wave propagation velocities which emerges as the eigenvalues of the mathematical model can be reproduced by the experiments, but discrepancies are found here as well. The first three reflected waves in the system are usually recorded with an equivalent frequency. As the waves continue to propagate through the system, the frequencies tend to increase slightly, giving deviations when compared to the calculations.

Verifying the presence of assumed theoretical phenomena, such as the precursor wave and boundary effects, has been more successful. Changing the boundary condition on the experimental rig gave suspected alterations to the recorded time-development. The precursor wave is also believed to be observed in the pressure measurement data, found as small disturbances in the overall behavior. An important factor in FSI is the presence of different wave propagation velocities, creating differences in frequency between the two subsystems. The strain should be excited earlier than the pressure, but this effect is not clearly observed in the measurement data.

Some modifications have also been implemented in an attempt to make the numerical more physically accurate, where the main effort have been to the boundary modeling. The implementation of a mass-spring-damper-model for the free-valve proved unsuccessful, producing numerical instability to the model. Incorporating a valve-closure characteristic gave better correlation with respect to pressure and strain amplitudes in the predictions.

7.1 Further Work

Since the validation of the numerical model were deemed somewhat inconclusive, further testing and validation of the computer program is necessary. If such experiments are to be conducted, efforts should be made to eliminate the vapor cavity problem by increasing the hydrostatic pressure and hence allowing for larger fluctuations to occur. The manual closure-mechanism should be changed with an automatic one that can obtain faster closing times, so more energy is contained in the system.

Measurements of several other parameters should also be considered. It would be interesting to quantify the shear forces during the transient. That way one can get increased the knowledge of the significance of this coupling mechanism, especially during the initial phase. To eliminate some of the uncertainty associated with the strain measurements, a gage in the circumferential direction should be added. This will give temperature compensation and also recorded hoop-strain. The linear strain gages could also be replaced with a rosette gage (two- or three legged strain gages) capable of sensing strain in the circumferential direction as well.

Some changes or addition to the numerical model should also be considered. Dependent on the experiment that will be used in an eventual validation-process, some more work should be done with the valve-closure model, as well as to the closure-function, making them more realistic. More thought should also be put into the domain discretization, and the effects of refining the spatial increment should be investigated. By doing this, the errors due to deviation between spatial nodes and measurement-points on the rig can be quantified.

BIBLIOGRAPHY

- [1] J. Hell. High flexible hydropower generation concepts for future grids. *Journal of Physics: Conference Series*, 813(1):012007, 2017.
- [2] J. Topiwala, G. Mistry, S. Patel, and P. Umrigar. Fluid structure interaction: Fundamentals and application - a review. *The International Journal of Research in Mechanical Engineering & Technology*, 6:65–68, May - Oct 2016.
- [3] B. Svingen. *Fluid Structure Interaction in Piping Systems*. NTNU, Trondheim, Norway, 1996. Ph.D Thesis.
- [4] A. S. Tijsseling. *Fluid-Structure Interaction in case of Waterhammer with Cavitation*. Communications on Hydraulic & Geotechnical Engineering, Delft University of Tech., The Netherlands, 1993. Report No. 93-6, Ph.D Thesis.
- [5] C. R. Nave. Wave speeds. <http://hyperphysics.phy-astr.gsu.edu/hbase/Sound/souspe2.html>. Georgia State University : Accessed: 05.12.2017.
- [6] E. B. Wylie and V. L. Streeter. *Fluid Transients in Systems*. Prentice Hall, Englewood Cliffs, NJ, USA, 1993.
- [7] A. S. Tijsseling, M. F. Lambert, A. R. Simpson, M. L. Stephens, J. P. Vítkovský, and A. Bergant. Skalák's extended theory of water hammer. *Journal of Sound and Vibration*, 310(3):718–728, 2008.
- [8] D. J. Williams. Waterhammer in non-rigid pipes: Precursor waves and mechanical damping. *Journal Mechanical Engineering Science*, 19(6):237–242, 1977.

-
- [9] R. Lakes. Meaning of poisson's ratio. <http://silver.neep.wisc.edu/~lakes/PoissonIntro.html>. University of Wisconsin : Accessed: 07.12.2017.
- [10] M. H. Chaudhry. *Applied Hydraulic Transients*. Springer, New York, NY, USA, 3. edition, 2014.
- [11] B. Brunone, U. M. Golia, and M. Greco. Effects of two-dimensionality on pipe transients modeling. *Journal of Hydraulic Engineering*, 121(12):906–912, 1995.
- [12] A. Bergant, A. S. Tijsseling, J. P. Vítkovský, D. I. C. Covas, A. R. Simpson, and M. F. Lambert. Parameters affecting water hammer wave attenuation, shape and timing - Part 1: Mathematical tools. *Journal of Hydraulic Research*, 46(3):373–381, 2008.
- [13] A. S. Tijsseling and A. G. T. J. Heinsbroek. The influence of bend motion on waterhammer pressures and pipe stresses. *Proc. of the 3rd ASME/JSME Joint Fluids Engineering Conf.*, July 1999. San Francisco, CA, USA.
- [14] D. Roylance. Pressure vessels, 2001. Lecture notes.
- [15] L. R. Hellevik. Cardiovascular biomechanics. Compendium in Biomechanics course at NTNU, Nov. 2015.
- [16] L. R. Hellevik. Numerical methods for engineers, a digital compendium. <http://folk.ntnu.no/leifh/teaching/tkt4140/>, 2017. Compendium in Numerical Methods course at NTNU.
- [17] Acromag Inc. Introduction to strain & strain measurements. *Technical Reference: White Paper*, 2001. Wixom, MI, USA.
- [18] Kulite Semiconductors. Product Advisor - HKM/HKL-233(X)-375(M). <https://www.kulite.com/products/product-catalog/miniature-high-pressure-pressure-transducer-hkm-hkl-233x-375-hkm-hkl-233x-375m-hkm-hkl-233x-375m/>. Accessed: 20180525.
- [19] HBM GmbH. LY Linear Strain Gauges with 1 Measuring Grid. <https://www.hbm.com/en/4561/ly-linear-strain-gauges-with-1-measurement-grid/>. Accessed: 20180525.
- [20] Brüel & Kjær A/S. Accelerometer - TYPE 4397. <https://www.bksv.com/en/products/transducers/vibration/Vibration-transducers/accelerometers/4397>. Accessed: 20180525.
- [21] B. W. Solemslie. Compendium in instrumentation, calibration & uncertainty analysis, 2010. NTNU, Trondheim, Norway.

-
- [22] Vishay Precision Group. Errors due to transverse sensitivity in strain gages. *Strain Gages and Instruments - Tech Note*, TN-509:91–99, 2011.
- [23] A. S. Tijsseling. Water hammer with fluid-structure interaction in thick-walled pipes. *Computers and Structures*, 85:844–851, 2007.
- [24] E. F. Toro. *Riemann Solvers and Numerical Methods for Fluid Dynamics*. Springer-Verlag, Berlin Heidelberg, 3. edition, 2009. Ch. 2, p. 42-85.
- [25] C. S. W. Lavooij and A. S. Tijsseling. Fluid-structure interaction in liquid-filled piping systems. *Journal of Fluids and Structures*, 5:573–595, 1991.
- [26] J. Gale. *Fluid-Structure Interaction for Simulations of Fast Transients*. University of Ljubljana, Ljubljana, Slovenia, 2008. Ph.D Thesis.
- [27] U. Karadžič, A. Bergant, and Petar Vukoslavčević. A novel pelton turbine model from water hammer analysis. *Strojniški vestnik - Journal of Mechanical Engineering*, 55(6):369–380, 2009.
- [28] W. Montero, R. Farag, V. Diaz, M. Ramirez, and B. L. Boada. Uncertainties associated with strain-measuring systems using resistance strain gauges. *Journal of Strain Analysis for Engineering Design*, 46(1):1–13, 2011.
- [29] Vishay Precision Group. Errors due to misalignment of strain gages. *Strain Gages and Instruments - Tech Note*, TN-511:107–111, 2010.
- [30] Vishay Precision Group. Errors due to Wheatstone bridge nonlinearity. *Strain Gages and Instruments - Tech Note*, TN-507-1:77–81, 2010.

NOMENCLATURE

GREEK

Symbol	–	Definition	Symbol	–	Definition
α	–	Pipe inclination angle	β	–	Misalignment angle
γ	–	Intended mounting angle	Δ	–	Discrete increment
ε_i	–	Pipe-wall strain	θ	–	Actual mounting angle
λ_i	–	System eigenvalue	ν	–	Poisson's ratio
ξ	–	Damping ratio	ρ_i	–	Mass density
σ_i	–	Pipe-wall stress	τ_0	–	Pipe-wall friction
τ	–	Dimensionless closing function	ψ	–	Pipe anchor coefficient
Ω	–	Electrical resistance, Ohm	ω_n	–	Natural frequency

ROMAN

Symbol	–	Definition	Symbol	–	Definition
D	–	Internal pipe diameter	E	–	Young's modulus
G	–	Gage factor	L	–	Pipe length
K	–	Fluid elastic modulus	L_G	–	Gage measuring length
P	–	Fluid pressure	Q	–	Fluid discharge
R_G	–	Gage resistance	R_I	–	Lead wire resistance
U	–	Gage output voltage	U_0	–	Gage output voltage, ε_0
U_{ex}	–	Excitation voltage	U_R	–	Voltage, relative
V	–	Fluid velocity		–	
c_i	–	Wave propagation velocity	e	–	Pipe-wall thickness
e_{x_i}	–	Uncertainty of x_i (abs)	e_q	–	Uncertainty of q (abs)
f_{x_i}	–	Uncertainty of x_i (rel)	f_q	–	Uncertainty of q (rel)
s_{x_i}	–	Standard deviation of x_i	$s_{x_i}^2$	–	Variation of x_i

u_i	–	Pipe-wall displacement	\dot{u}_i	–	Pipe-wall velocity
\ddot{u}_i	–	Pipe-wall acceleration	$v_{i,1}$	–	Relative valve opening
x_i	–	Measurand i	\bar{x}_i	–	Mean of x_i

SUBSCRIPTS

Symbol	–	Definition	Symbol	–	Definition
f	–	Fluid property	s	–	Structural property
z	–	Axial component	ϕ	–	Circumferential component
r	–	Radial component	*	–	Design quantity
0	–	Steady state			

ABBREVIATIONS

Symbol	–	Definition	Symbol	–	Definition
FBD	–	Free-body-diagram	FSI	–	Fluid-structure interaction
MOC	–	Method of characteristics	FSO	–	Full Scale Output
RHS	–	Right-hand-side	RSS	–	Root-sum-square

APPENDIX A

ADDITIONAL RESULTS

Some additional results are given in this chapter. The following figures will show a selection of both measurement data, calculated response from the computer code and some additional comparison between the two.

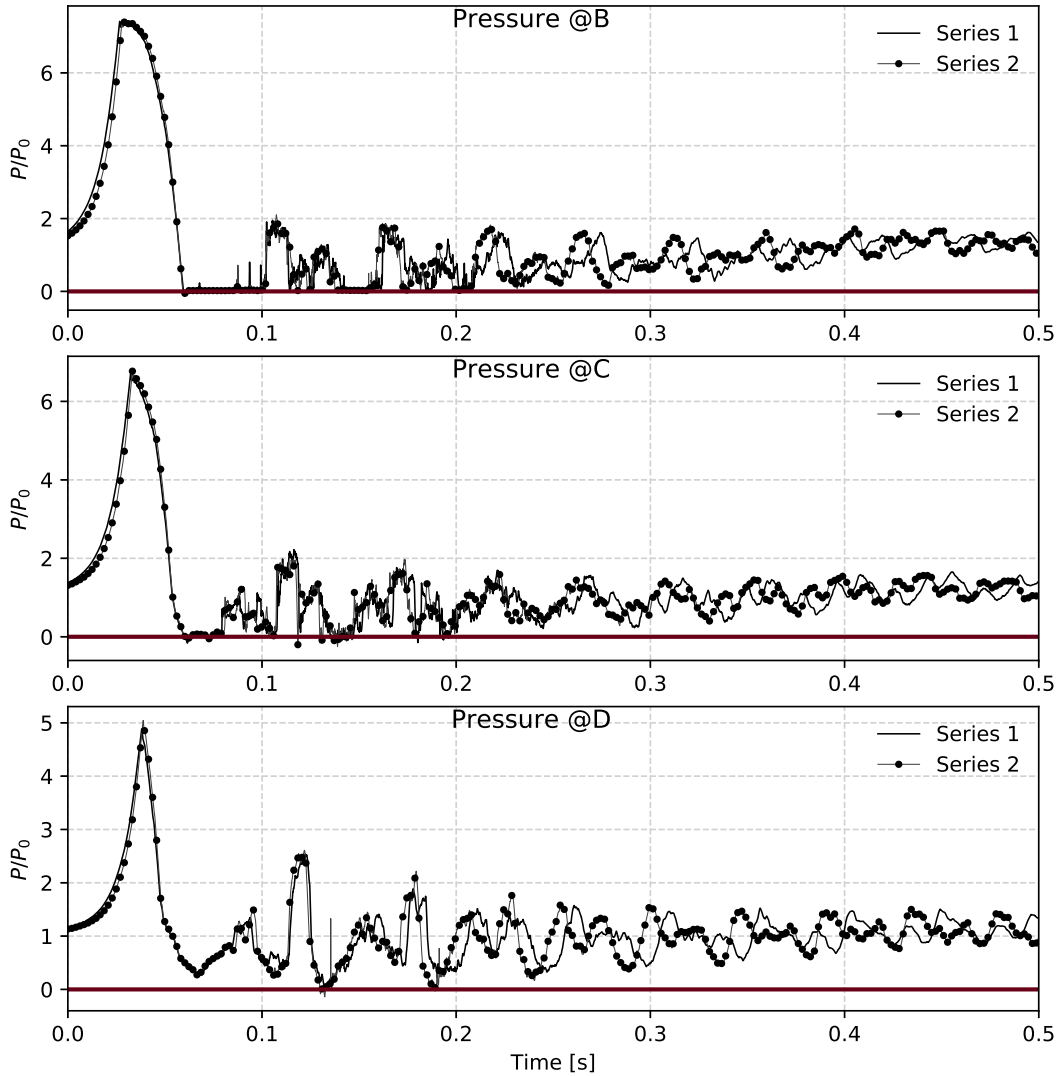


Figure A.1: Pressure-time behavior of the pressure transducers at $V_0 = 0.980$ m/s. Showing first 0.5 s of the transient. Red line indicates $P = 0$. Series 1 and 2 are obtained only minutes apart.

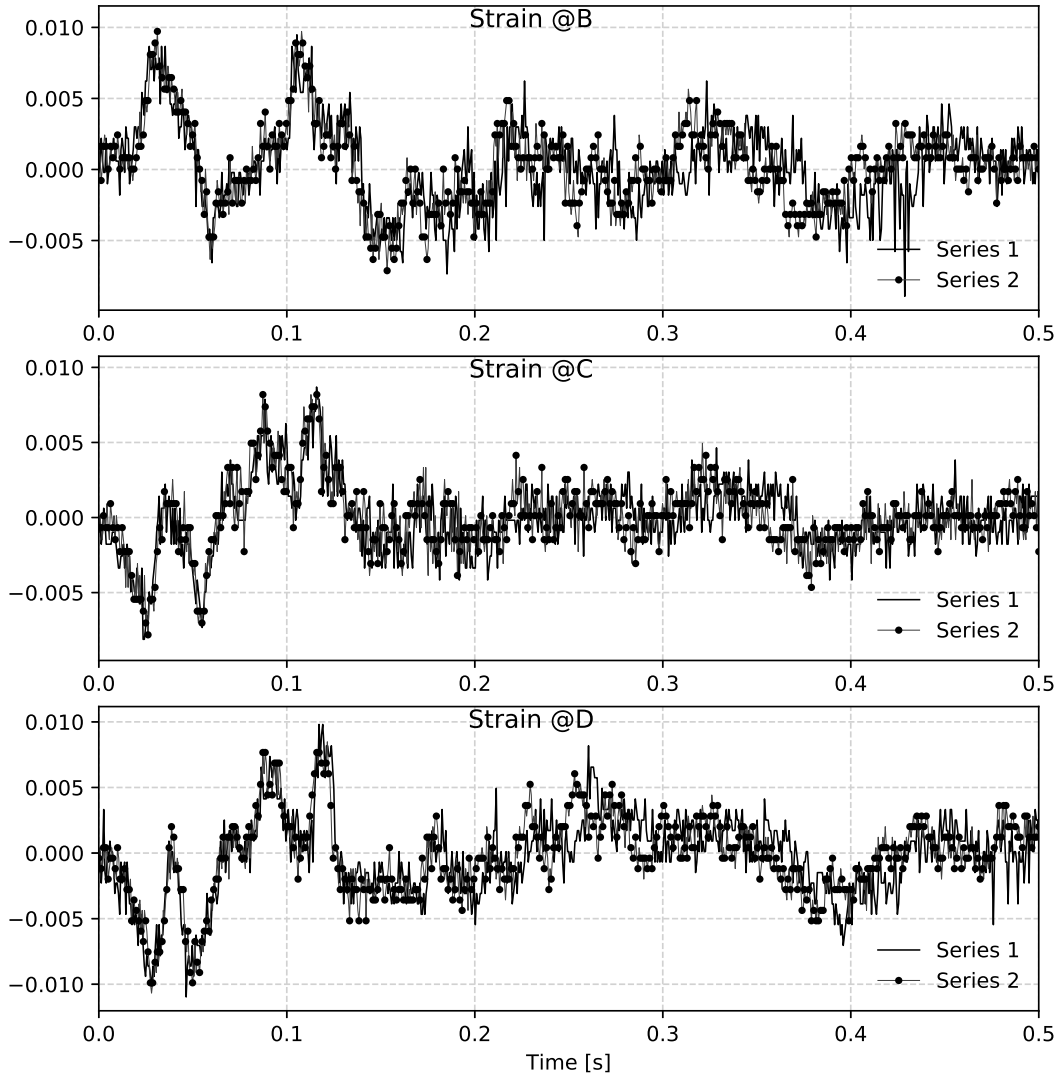


Figure A.2: Pressure-time behavior of the pressure transducers at $V_0 = 0.980$ m/s. Showing first 0.5 s of the transient. Red line indicates $P = 0$. Series 1 and 2 are obtained only minutes apart.

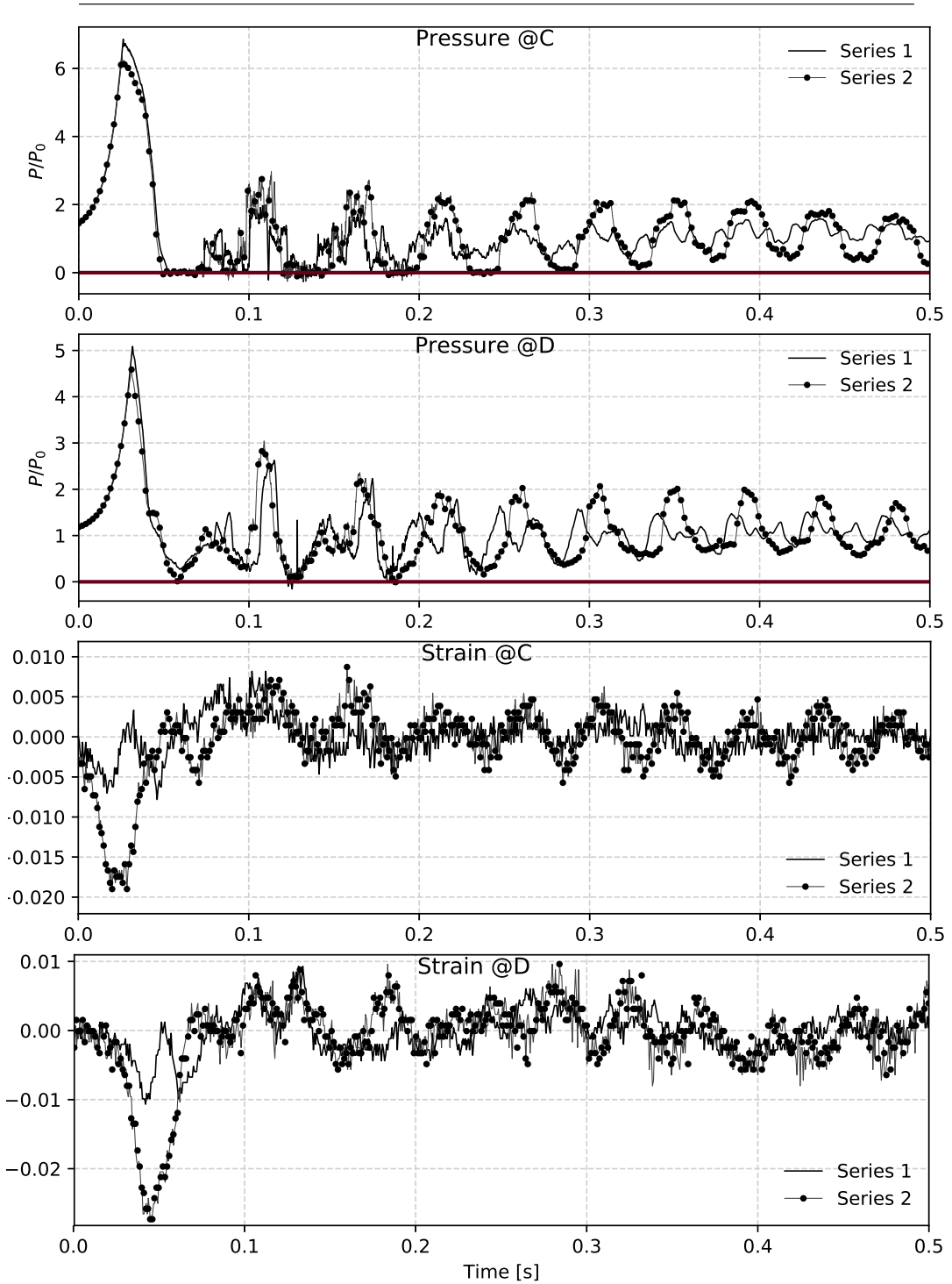


Figure A.3: Comparison of boundary conditions for the experimental rig at measurement-points C and D. Series 1: Fixed valve, Series 2: Detached valve. $V_0 = 0.980$ m/s

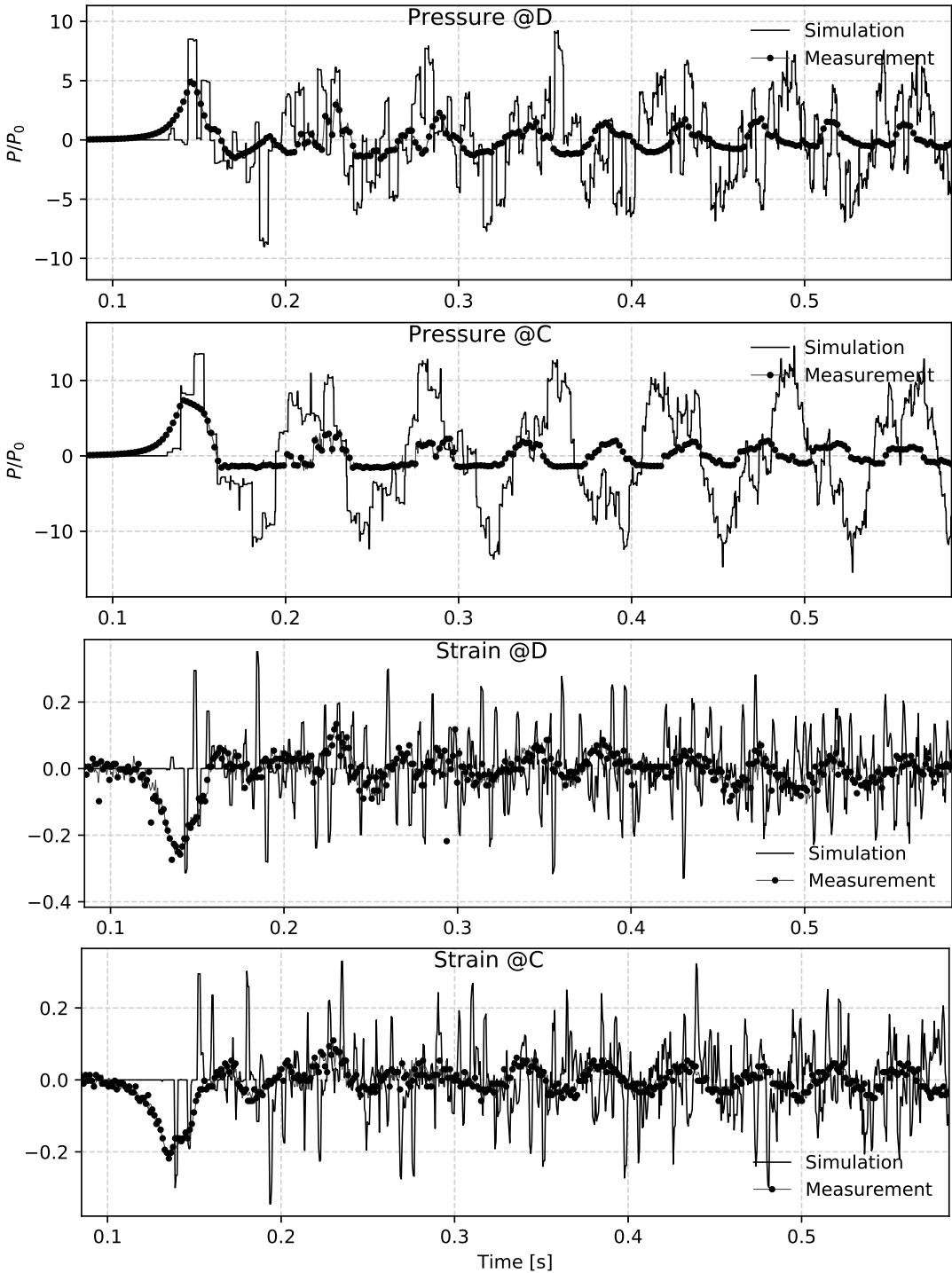


Figure A.4: Measurements against calculated response with a free, massless valve boundary condition with $t_c = 0$. $V_0 = 0.980$ m/s

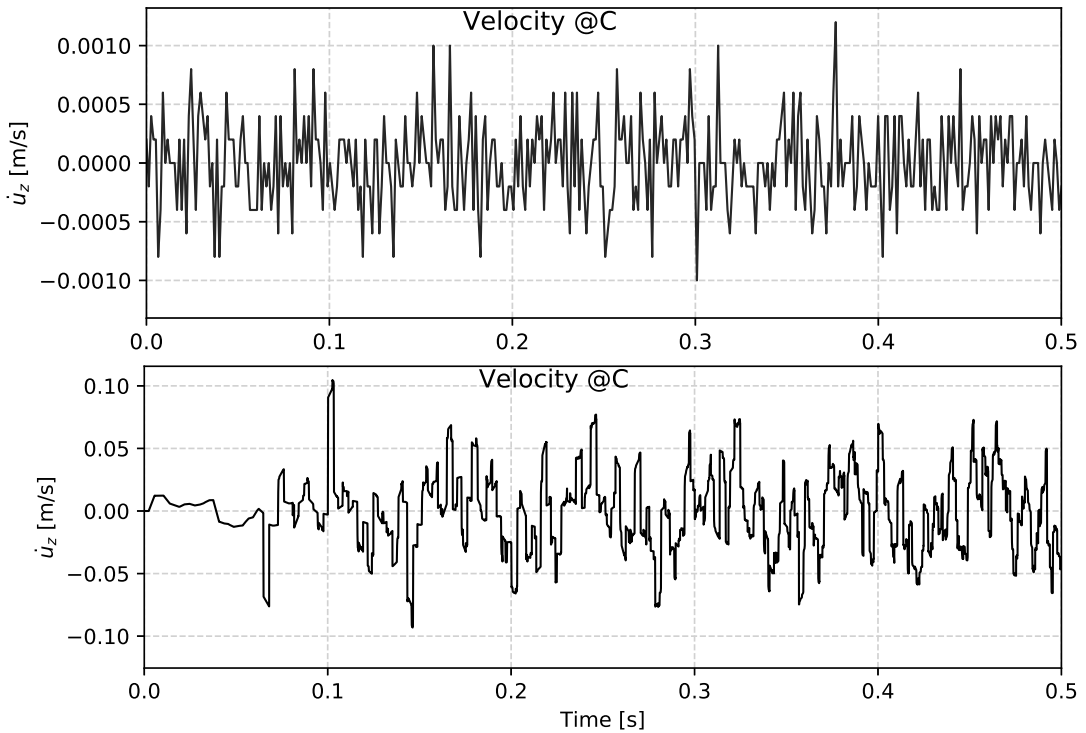


Figure A.5: Showing a representative derived response compared to simulation for the axial displacement velocity, \dot{u}_z . $V_0 = 0.980$ m/s. Notice the differences in magnitude between the prediction from the computer program and the derived response from the measurements.

APPENDIX B

UNCERTAINTY ANALYSIS AND CALIBRATION

The following chapter include some of the features that are necessary in an uncertainty analysis, such as relevant equations from calculating specific uncertainties and some regression analysis plots.

B.1 Relevant equations for the Uncertainty Analysis

The following equations and relationships are used in the uncertainty analysis in section 3.2. They are included here for the sake of completeness.

B.1.1 Pressure measurements

The t-distribution The t-distribution is used in uncertainty analysis of finite measurements series that are assumed to approximate a normal distribution as a series size gets larger. It is usually be used to find the random uncertainty of, and is estimated using the following relationship

$$f_{x_i} = \pm t_{\alpha/2} \frac{s_{x_i}}{\sqrt{n}} \quad (\text{B.1})$$

where

$$s_{x_i} = \left[\frac{1}{n-1} \sum_{i=1}^n (x_i - \bar{x}_i)^2 \right]^{1/2}$$

and $t_{\alpha/2}$ is a tabulated value dependent on the size, n [21]. The values used for the regression- and steady-analysis was $t_{\alpha/2} = 2.08$, $n = 21$ and $t_{\alpha/2} = 1.96$, $n > 1000$, respectively.

Repeatability error Something on repeatability error , describe what to look for, why this can be used for dynamic measurements as a substitution when static calibration is used.

B.1.2 Strain measurements

Misalignment error The misalignment error has it's origin in the installation process. Any error, say β , between the measurement intended angle, γ and the actual mounted gage's sensing angle, θ , will make the gage read the strain along a slightly different axis than the intended. The actual angle can therefore be expressed as $\theta = \gamma \pm \beta$. For the measurement done here, the intended axis is the axial, z . A proposed estimate for this error is

$$e_{s_m} = \varepsilon_{z \pm \beta} - \varepsilon_z \quad (\text{B.2})$$

where ε_z and $\varepsilon_{z \pm \beta}$ is the measured strain at the intended angle and misaligned angle, respectively [28].

Using Mohr's circle, assuming a uniaxial stress field, i.e. $\sigma_z, \sigma_\phi \neq 0$, the error can written as

$$e_{s_m} = \frac{1}{2}(\varepsilon_p - \varepsilon_q)(\cos 2(\phi \pm \beta) - \cos 2\phi) \quad (\text{B.3})$$

or normalized with respect to intended strain

$$f_{s_m} = \frac{\cos 2(\phi \pm \beta) - \cos 2\phi}{\frac{R_\varepsilon + 1}{R_\varepsilon - 1} + \cos 2\phi} \quad (\text{B.4})$$

Substituted in for the relevant intended and misaligned angles, f_{s_m} is the relative misalignment uncertainty for the strain measurements. [29].

Transverse sensitivity Due to the material contraction factor, ν , change in distance between points on a specimen will result in an opposite change in the perpendicular direction. This will influence the strain readings, and the gage's resistance to this unwanted change is called the transverse sensitivity. The error this introduce to the measurements is given by

$$e_{s_t} = \frac{K_t \left(\frac{\varepsilon_\phi}{\varepsilon_z} + \nu_G \right)}{1 - \nu_G K_t} \quad (\text{B.5})$$

where K_t is the transverse sensitivity coefficient and ν_G the contraction factor for the material which was used to find the gage factor. The ε_ϕ and ε_z is "measured" transverse and axial strains [28]. Since only one strain gage was used for each bridge, the stress-strain

relation can be used to find the transverse strain related to the measurements. In the two relevant directions, z and ϕ , they are given as

$$\varepsilon_z = \frac{1}{E}(\sigma_z - \nu\sigma_\phi) \quad \varepsilon_\phi = \frac{1}{E}(\sigma_\phi - \nu\sigma_z) \quad (\text{B.6})$$

Here a plane stress situation is assumed, giving $\sigma_r = 0$ [4].

Temperature error INCLUDE MORE DETAIL, so it can be comfortably be neglected. These errors come from the fact that changing temperatures will influence the resistance of the gage due to the thermal expansion or contraction of the measuring grid. The gage factor will also be effected by the same mechanisms. The estimated error from the change in temperature can be found using

$$e_{s_T} = \varepsilon_z - \frac{G_I(\varepsilon_z - \varepsilon_{z_T})}{G_i[1 + C_T(T - T_F)]} \quad (\text{B.7})$$

where G_i is the gage factor at room temperature and G_I the instrumentation gage factor. T is the temperature during the tests and C_T is the variation coefficient for the gage factor at T . T_f is the reference temperature for C_T . ε_{z_T} is the temperature induced strain [28].

Bridge nonlinearity error Nonlinearity in the Wheatstone bridge comes from the fact that as the gage is put under tension (or contraction), the resistance changes, making the circuit unbalanced, and hence the voltage output a nonlinear function of this resistance change. For applications with small measured strains¹, these errors is usually of negligible magnitude. If they are to be included, the error can be estimated using

$$e_{s_n} = \frac{2\varepsilon_z}{2 - G\varepsilon_z} \quad (\text{B.8})$$

where ε_z is the measured strain and G is the gage factor [30].

B.2 Pressure Transducer Regression Curves

The obtained regression curves for the pressure transducer calibration is given in figure B.1. Notice that the range of calibration was from 1 – 10 bar, using 23 points. The full reports from the calibration can be found in the digital attachment associated with this thesis.

¹ This is usually the case when the specimen material is a metal.

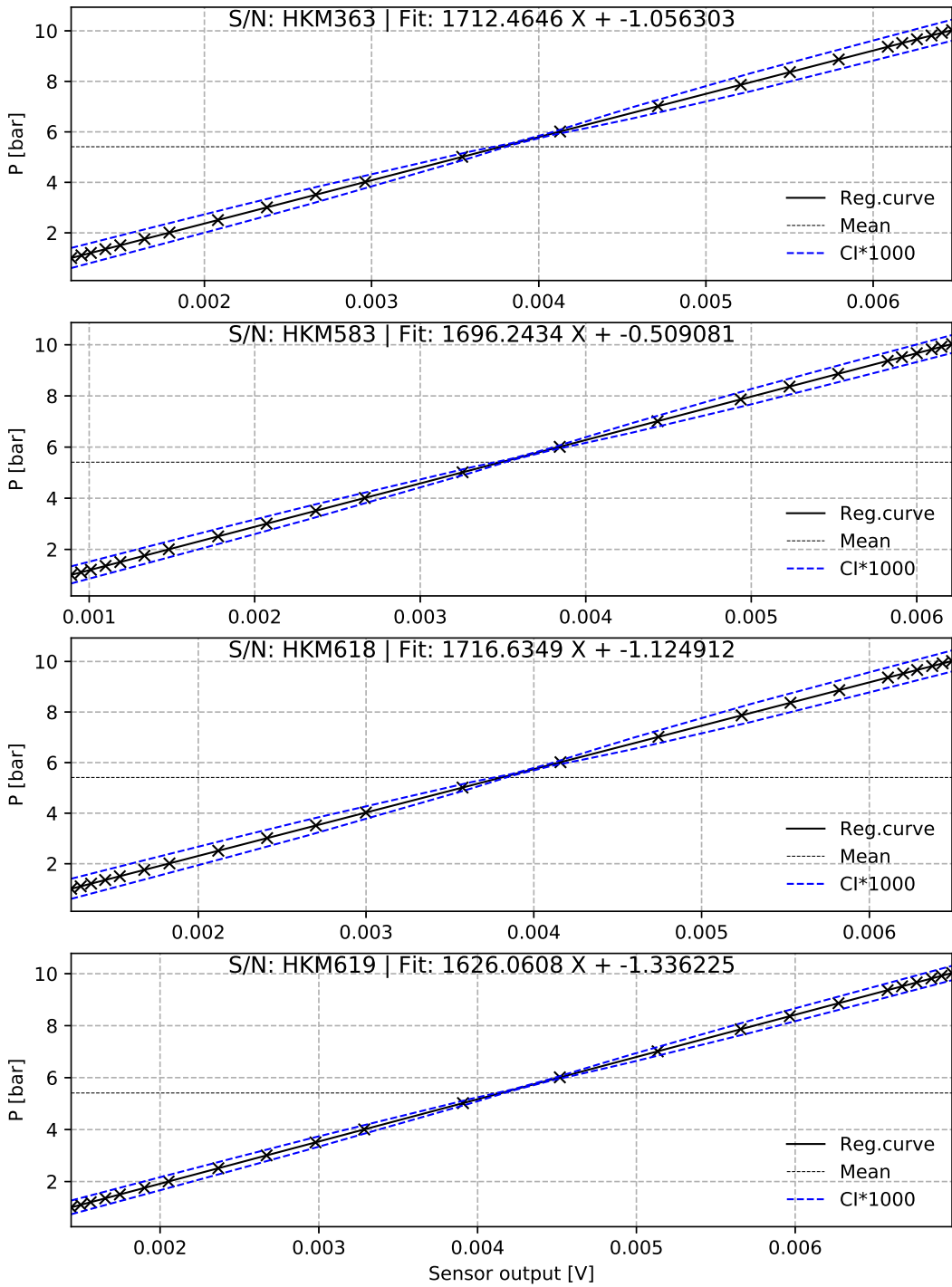


Figure B.1: Regression curves from calibration of the pressure transducers

APPENDIX C

RISK ASSESSMENT REPORT

The risk assessment-report from the planning of this study's laboratory activities can be found in the following pages. Given the nature of the activities, only a few hazardous factors were identified. The full laboratory risk assessment and safe-job-analysis can be found in the digital attachment associated with this thesis.

NTNU	Hazardous activity identification process			Prepared by	Number	Date
				HSE section	HMSRVZ901E	08.01.2013
HSE				Approved by	The Rector	
						

Unit: Department of Energy and Process Engineering

Date: 08.06.2018

Line manager: Terese Løvås

Participants in the identification process: Supervisor: Bjørnar Svingen, Student: Anders Thorstad Bø

Short description of the main activity/main process: Master project for: Anders Thorstad Bø. Fluid-Structure Interaction in a Pipe

Is the project work purely theoretical? (YES/NO): NO

Answer "YES" implies that supervisor is assured that no activities requiring risk assessment are involved in the work. If YES, briefly describe the activities below. The risk assessment form need not be filled out.

Signatures: Responsible supervisor: *Bjørnar Svingen* Student: *Anders Thorstad Bø*

ID nr.	Activity/process	Responsible person	Existing documentation	Existing safety measures	Laws, regulations etc.	Comment
1	Measurements on a waterhammer-rig at the Waterpower Laboratory	Anders Thorstad Bø	See Riskovurderingsrapport attached to thesis	See: Riskovurderingsrapport attached to thesis	See Riskovurderingsrapport attached to thesis	

NTNU	Risk assessment		Prepared by	Number	Date
HSE/MS			HSE section	HMSTRV/2803E	04.02.2011
			Approved by	Replaces	
			The Rector	01.12.2008	

Unit: Department of Energy and Process Engineering

Date: 08.06.2018

Line manager: Terese Løvås

Participants in the identification process: Supervisor: Bjørnar Svingen, Student: Anders Thorstad Bø

Short description of the main activity/main process: Master project for: Anders T. Bø: Fluid-Structure Interaction in a Pipe

Signatures: Responsible supervisor:

Bjørnar Svingen

Student:



Anders Thorstad Bø

Activity from the identification process form	Potential undestriable incidents/strain	Likelihood: (1-5)	Consequence:			Risk Value (Human)	Comments/status Suggested measures
			Human (A-E)	Environment (A-E)	Economy/ material (A-E)		
1.	Pipe-burst	1	C	A	C	C1	
1.	Waterleakage from cracks/bad fittings	2	A	A	B	A2	
1.	Physical harm due to significant pipe-motion	1	C	A	B	C1	

- Likelihood, e.g.:
1. Minimal
 2. Low
 3. Medium
 4. High
 5. Very high

- Consequence, e.g.:
- A. Safe
 - B. Relatively safe
 - C. Dangerous
 - D. Critical
 - E. Very critical

Risk value (each one to be estimated separately):
 Human = Likelihood x Human Consequence
 Environmental = Likelihood x Environmental consequence
 Financial/material = Likelihood x Consequence for Economy/material

NTNU		Prepared by		Number		Date	
		HSE section		HMSRV2803E		04.02.2011	
HSE/KS		Approved by				Replaces	
		The Rector				01.12.2006	
Risk assessment							

Potential undesirable incident/strain

Identify possible incidents and conditions that may lead to situations that pose a hazard to people, the environment and any materiel/equipment involved.

Criteria for the assessment of likelihood and consequence in relation to fieldwork

Each activity is assessed according to a worst-case scenario. Likelihood and consequence are to be assessed separately for each potential undesirable incident. Before starting on the quantification, the participants should agree what they understand by the assessment criteria:

Likelihood		Low		Medium		High		Very high	
1		2		3		4		5	
Once every 50 years or less		Once every 10 years or less		Once a year or less		Once a month or less		Once a week	
Consequence									
Grading		Human		Environment		Financial/materiel			
E Very critical		May produce fatality/fes		Very prolonged, non-reversible damage		Shutdown of work > 1 year.			
D Critical		Permanent injury, may produce serious serious health damage/sickness		Prolonged damage. Long recovery time.		Shutdown of work 0.5-1 year.			
C Dangerous		Serious personal injury		Minor damage. Long recovery time		Shutdown of work < 1 month			
B Relatively safe		Injury that requires medical treatment		Minor damage. Short recovery time		Shutdown of work < 1week			
A Safe		Injury that requires first aid		Insignificant damage. Short recovery time		Shutdown of work < 1day			

The unit makes its own decision as to whether opting to fill in or not consequences for economy/materiel, for example if the unit is going to use particularly valuable equipment. It is up to the individual unit to choose the assessment criteria for this column.

Risk = Likelihood x Consequence
Please calculate the risk value for "Human", "Environment" and, if chosen, "Economy/materiel", separately.

About the column "Comments/status, suggested preventative and corrective measures":
Measures can impact on both likelihood and consequences. Prioritise measures that can prevent the incident from occurring. In other words, likelihood-reducing measures are to be prioritised above greater emergency preparedness, i.e. consequence-reducing measures.

NTNU		Risk matrix		Prepared by	Number	Date
				HSE Section	HMSRVZ804	8 March 2010
HSE/KS				approved by	Page	Replaces
				Reactor	4 of 4	9 February 2010

MATRIX FOR RISK ASSESSMENTS at NTNU

		CONSEQUENCE				
		Extremely serious	E1	E2	E3	E4
Not significant	Extremely serious	E1	E2	E3	E4	E5
	Serious	D1	D2	D3	D4	D5
	Moderate	C1	C2	C3	C4	C5
	Minor	B1	B2	B3	B4	B5
	Very low	A1	A2	A3	A4	A5
		Very low	Low	Medium	High	Very high
		LIKELIHOOD				

Principle for acceptance criteria. Explanation of the colours used in the risk matrix.

Colour	Description
Red	Unacceptable risk. Measures must be taken to reduce the risk.
Yellow	Assessment range. Measures must be considered.
Green	Acceptable risk Measures can be considered based on other considerations.

APPENDIX D

CRHT-VIII CONFERENCE PAPER

The following paper was written by the author as a contribution to the *8th International symposium on Current Research in Hydraulic Turbines at Kathmandu University, 20. March 2018.*

It focuses on the mathematical modeling and simulation of the waterhammer-event in a pipe. It is a compact version of the authors work done of the subject during the fall of 2017. It also presents the planned experiments for the validation and verification of the computer program written as a part of that work.

Fluid-structure interaction in a pipe

Anders Thorstad Bø¹ and Bjørnar Svingen¹

¹ Department of Energy and Process Engineering, Norwegian University of Science and Technology, Trondheim, Norway

E-mail: anderstb@stud.ntnu.no

Abstract. The investigation of fluid-structure interaction (FSI) in piping systems during transient events call for numerical modeling in order to accurately capture the rapid fluctuations of the model variables. The ability to predict the forces and movement of such systems will help better understand the mechanisms responsible for the characteristic transient behavior. For simple systems, the method of characteristics (MOC) is one of the most popular modeling approaches, mainly due to rapid execution times and the almost analytical solution that can be obtained. This paper will deal with numerical and experimental investigation of a waterhammer-event. The extended waterhammer equations are used to describe a straight pipe with arbitrary boundary conditions, and the MOC-transformed version was implemented numerically to solve a reservoir-pipe-valve system. An experimental study of the same setup at NTNU's Waterpower Laboratory is to be conducted in order to validate the predictions made by the computer program. Measurements for pressure, strain and acceleration of the pipe system will be analyzed and compared to the numerical results, to further pinpoint the advantages and shortcomings of the MOC-procedure.

Keywords: Fluid-structure interaction, waterhammer, method of characteristics, experimental study

1. Introduction

In the process of designing fluid piping systems, accurate prediction of the potential and expected forces on the structure and its components is an important part of the development process. In the case of closed conduit flows, one of the most extreme and possibly devastating events to account for is a pressure surge. These happen when a steady flow is jolted out of this state due to sudden changes in the system parameters. These events are always unsteady and results in significant, internal pressure fluctuations. To capture the entire picture of the system behavior during a pressure surge, it is important to take into account how the drops and rises of fluid pressure influence the surrounding structure. Studying the fluid-structure interaction (FSI) in these systems will broaden the understanding of the conduit's role in the characteristic behavior of pressure surges. Numerical or experimental considerations are vital, mainly due to the rapidness and complexity of the motion of both domain's parameters.

This paper will give a brief explanation of relevant background material for understanding fluid-structure interaction in water-filled pipes. Then a numerical approach utilizing the method of characteristics (MOC) to transform Skalak's four-equation model, the extended waterhammer equations, to a set of linear, ordinary differential equations will be presented. Numerical results from this model on a reservoir-pipe-valve system will also be discussed. Lastly, the numerical model is to be validated experimentally, so here, the apparatus, instrumentation and method will be explained.

2. Theoretical background

2.1. FSI-definitions

A definition of fluid-structure interaction is the dynamic and coupled interaction between a fluid and a structure. When two or more subsystems are interconnected, a change in one is then assumed to result in a response for the others, which in turn will yield a new response in the first. This interaction can be a result an external flow over a solid structure, such as air flow past a wind turbine, or a fluid confined inside a structure, such as a water pipe [1].

It is common to classify these systems as weakly or strongly coupled. This is based on the magnitude of the response from a subsystem as other subsystems alter their state. This is especially important when a system is to be modeled mathematically, because a weak coupling usually simplifies the modeling requirements drastically [1].

Furthermore, two different numerical approaches exists, namely a partitioned and a monolithic approach. When using the former, the subsystems are considered individually, meaning that the governing equations for the different systems can be solved separately. Using a suited interface, information is transfered between the domains. This gives the opportunity to use existing algorithms. A drawback is the fact that such an explicit interface will give rise to numerical errors. Algorithms modification is therefore necessary to increase model accuracy. A monolithic approach, on the other hand, treats the subsystems as one, single system. The interface, or coupling, is implicitly incorporated into the system equations, increasing accuracy directly. A consequence of this is the need for a specialized numerical equation for each system investigated [1].

2.2. Waterhammer

A pressure surge or waterhammer, as it is usually denoted in fluid piping applications, occur when a steady system undergo a sudden disturbance or change in one or more of it's parameters. Examples of this change in state are sudden pump start-ups, load rejection from turbines and sudden valve closures. Common for the previous examples are a change in the fluid velocity, which results in a significantly changed fluid pressure [2]. In fluid-pipe-systems a strong coupling exists, so the altered internal pressure will drastically influence the surrounding pipe.

2.2.1. Wave propagation velocity Essential for understanding the effect waterhammer-events will have on different piping systems is the wave propagation through the different media. The following expression can be found for the constrained fluid wave propagation velocity

$$c_f = \left[\frac{K}{\rho_f} \left(1 + \psi \frac{DK}{eE} \right)^{-1} \right]^{1/2} \quad (2.1)$$

with K and E as the modulus of elasticity for the fluid and pipe-wall material, ρ_f , D and e as mass density of the fluid, pipe diameter and pipe-wall thickness. ψ is a scaling factor accounting for the pipe anchoring and is dependent on Poisson's ratio. The development of equation (2.1), along with multiple versions of ψ can be found in [2,3]. The wave propagation velocity of the surrounding structure is can be found as

$$c_s = \sqrt{\frac{E}{\rho_s}} \quad (2.2)$$

through direct substitution of the general equation for wave propagation in any elastic medium [4]. The above equations hold when the pressure and axial stress waves can be taken as the dominating wave propagation modes, which is the case when long wavelengths relative to pipe radius is assumed. For most practical systems the pressure wave, c_f , is also assumed slower than axial stress wave, c_s . [3].

2.2.2. Domain coupling An important concept in FSI-considerations is how the domains are coupled. At the starting-point of a waterhammer, the increased fluid pressure will cause the pipe-wall to expand or contract radially, resulting in two propagating waves, one pressure and one axial stress wave. Due to the material contraction factor or Poisson's ratio, ν , the pipe upstream and downstream of this changed pressure will react with an equal, but opposite, contraction or expansion, resulting in a changing fluid pressure. Since this represents a new change in the system conditions, another faster, but weaker wave is produced, known as a precursor wave. This indicates a strong coupling, significantly altering the entire system behavior, often attributed as the Poisson coupling [5].

A different coupling effect can be found at connecting points between a length of pipe and another system component. Most relevant for the applications presented here is a terminal component, i.e. a valve or orifice. As a pressure force acts on a closed valve, and the system is allowed to move axially, forces inside the pipe-wall will act in the opposite direction with mutual strength. This dynamic interaction between the the two domains at specific locations is known as a junction coupling, and will be shown to also alter the system behavior drastically [3].

2.3. The extended waterhammer equations

The following section will present the four-equation model or extended waterhammer equations used to model the straight reservoir-pipe-valve. The model is derived from the fluid continuity and momentum equations along with the two-dimensional equation of structural motion in cylindrical coordinates. Important assumptions to note is axial symmetry, small structural deformations, negligible convective terms in both domains¹ and long wavelengths. The last assumption is what gives a one-dimensional model in the end. For a more thorough description, see [3]. The resulting four-equation model can be written as

Fluid equations

$$\frac{\partial V}{\partial t} + \frac{1}{\rho_f} \frac{\partial P}{\partial z} = -f \frac{V_{rel}|V_{rel}|}{4R} \quad (2.3)$$

$$\frac{\partial V}{\partial z} + \frac{1}{\rho_f c_f^2} \frac{\partial P}{\partial t} = 2\nu \frac{\partial \dot{u}_z}{\partial z} \quad (2.4)$$

Pipe equations

$$\frac{\partial \dot{u}_z}{\partial t} - \frac{1}{\rho_s} \frac{\partial \sigma_z}{\partial z} = f \frac{\rho_f A_f V_{rel}|V_{rel}|}{\rho_s A_s 4R} \quad (2.5)$$

$$\frac{\partial \dot{u}_z}{\partial z} - \frac{1}{\rho_s c_s^2} \frac{\partial \sigma_z}{\partial t} = -\frac{\nu R}{eE} \frac{\partial P}{\partial t} \quad (2.6)$$

where c_f^2 and c_s^2 are the wave propagation speeds for the fluid and pipe-wall (see equations (2.1) and (2.2)). The four dependent variables, V, P, \dot{u}_z and σ_z are all averaged across the pipe's inner radius and pipe-wall thickness. The terms on the LHS of equations (2.3) and (2.5) is the steady shear stress accounting for the friction forces between the fluid and pipe-wall. It is modeled using Darcy-Weisbach friction factor and a steady state force balance of a fluid-filled pipe. The term $V_{rel} = V - \dot{u}_z$ accounts for the difference between the two velocities.

The coupling between the domains can clearly be seen in the above equations through the presence of Poisson's ratio. Pressure and axial stress is added as a source and sink term to their respective equations. In this way, it is easy to see what happens for $\nu = 0$. The terms vanish, and consequently decouples the domains.

¹ This is due to the fact that the fluid and structural velocities are much smaller than the wave propagation velocities, i.e. $c_f \gg u, c_s \gg \dot{u}_z$

2.4. Method of characteristics

In general, a set of linear partial differential equations (PDE) will be classified through their characteristics. These are the lines or curves in the domain along which information of the solution travel. The shape of these characteristics are decided by the system eigenvalues. In turn, this will allow the set to be classified as either elliptic, parabolic or hyperbolic. Finding the eigenvalues as real and distinct, the system is hyperbolic, making the method of characteristics applicable [6].

Consider an arbitrary set of hyperbolic PDE's given as

$$\frac{\partial \mathbf{u}(x, t)}{\partial t} + \mathbf{R} \frac{\partial \mathbf{u}(x, t)}{\partial x} = \mathbf{f}(x, t) \quad (2.7)$$

where \mathbf{u} and \mathbf{f} is the variable and forcing term vector, respectively. \mathbf{R} are the system matrix. With m real, distinct eigenvalues, the system will also have m linearly independent eigenvectors which can be combined into a matrix, \mathbf{K} . If \mathbf{R} is considered diagonalizable, the relation, $\mathbf{R} = \mathbf{K}\mathbf{\Lambda}\mathbf{K}^{-1} \Rightarrow \mathbf{\Lambda} = \mathbf{K}^{-1}\mathbf{R}\mathbf{K}$ makes it possible to define a new dependent variables as

$$\mathbf{w}(x, t) = \mathbf{K}^{-1}\mathbf{u}(x, t) \quad (2.8)$$

which consequently decouples the system in equation (2.7). Multiplication of \mathbf{K}^{-1} and substitution of \mathbf{w} yields

$$\frac{\partial \mathbf{w}(x, t)}{\partial t} + \mathbf{\Lambda} \frac{\partial \mathbf{w}(x, t)}{\partial x} = \mathbf{K}^{-1}\mathbf{f}(x, t) \quad (2.9)$$

which is the characteristic form of the original PDE.

The method of characteristics then considers the system along m characteristic curves that follow the ODE

$$\frac{dx}{dt} = \lambda_i \quad (2.10)$$

where λ_i is the system eigenvalues. Using this ODE, one can further simplify equation (2.9) to a set of linear, ordinary differential equations on the form

$$\frac{d\mathbf{w}(x, t)}{dt} = \mathbf{K}^{-1}\mathbf{f}(x, t) \quad (2.11)$$

known as the compatibility equations of equation (2.7). Integration forward in time will then gives a system of m equations which can be solved numerically [7].

3. Numerical implementation

The transformation procedure of the extended waterhammer equations, including its discretization, will generally follow the work done by Tijsseling in [3], with a few minor exceptions.

3.1. MOC-transformation

The MOC-procedure briefly explained in above can be used directly on the system

$$\mathbf{A} \frac{\partial \mathbf{y}}{\partial t} + \mathbf{B} \frac{\partial \mathbf{y}}{\partial z} = \mathbf{r} \quad (3.1)$$

which is the four-equation model rewritten in matrix form. This equation has four distinct, real eigenvalues that will be denoted

$$\lambda_{1,2} = \pm \tilde{c}_f, \quad \lambda_{3,4} = \pm \tilde{c}_s \quad (3.2)$$

Here λ_i corresponds to wave propagation velocities that are slightly altered from the theoretical presented in section 2.2.1. The alteration is a result of the domain coupling. In fact, the system eigenvalues equal the theoretical wave velocities if $\nu = 0$.

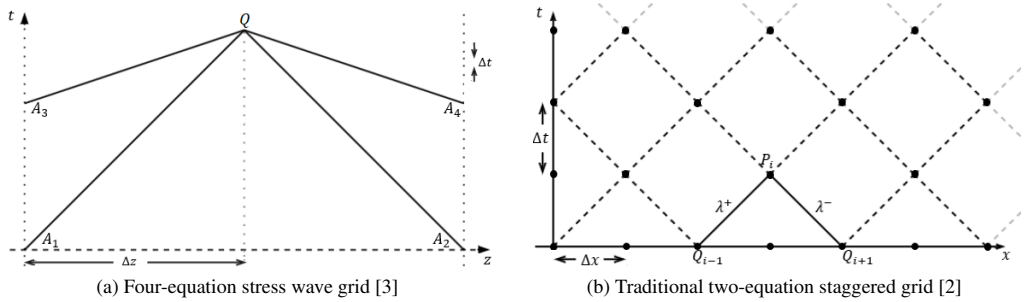


Figure 1: Graphical representation of the MOC for a two- and four-equation system

With $\mathbf{R} = \mathbf{A}^{-1}\mathbf{B}$ and $\mathbf{K}^{-1} = \mathbf{T}\mathbf{A}$, the new dependent variable

$$\mathbf{v} = \mathbf{T}\mathbf{A}\mathbf{y} \quad \text{or} \quad v_i = (\mathbf{T}\mathbf{A})_{ij}y_j \quad , \quad i = 1, 2, 3, 4 \quad (3.3)$$

can be defined, giving a decoupled set of equations as

$$\frac{\partial v_i}{\partial t} + \lambda_i \frac{\partial v_i}{\partial z} = (\mathbf{T}\mathbf{r})_i \quad , \quad i = 1, 2, 3, 4 \quad (3.4)$$

The matrix \mathbf{T} is a transformation matrix found by solving the equation $\mathbf{T}\mathbf{B} = \mathbf{A}\mathbf{T}\mathbf{A}$ for \mathbf{T} . The details of that solution can be found in [3].

Evaluation of equation (3.4) along lines λ_i gives the system compatibility equations. Considering the case where $\mathbf{r} = \mathbf{0}$, the linear case can be obtained as

$$(v_i)_Q = (v_i)_{A_i} \quad , \quad i = 1, 2, 3, 4 \quad (3.5)$$

Practical applications of MOC require this discretization in time and space. Most common is to choose a fixed value for either dx or dt , then calculate the other using a discrete version of equation (2.10). One choice is shown graphically in figure 1a, where $\lambda_i = \tilde{c}_s$, the so-called stress-wave grid [3]. The two-equation case is shown in figure 1b to highlight the similarity and differences between the traditional staggered grid used for fluid transient applications and the grid used here.

Because $\tilde{c}_s > \tilde{c}_f$, the characteristics corresponding to the pressure waves will have a different slope than the axial stress waves. When solving a set of equations numerically with MOC, information about the solution travel along lines $A_i \rightarrow Q$, carrying the solution from one point back in time to the present time-step. To make sure A_i actually are grid-points, thus avoiding a need for interpolation, refinement of the temporal grid-spacing is necessary with the current configuration. A method proposed in [8] is a wave velocity adjustment. This is done by approximating the ratio \tilde{c}_s/\tilde{c}_f to a rational number, say b/a . It must be noted that adjustment of the wave velocities are done by altering the physical constants that c_f and c_s depend on. The method used here alters the two mass densities. The actual numbers then decide how far the characteristic lines must reach back in time to obtain information of the solution.

3.2. Boundary conditions

The numerical discretization in this study has been chosen because it avoids the need for interpolation at the domain boundaries. For Q_i on the upstream or downstream boundary, only two of the four

characteristics are available. In order to solve the system four boundary conditions must be specified. Using the upstream case as an example, consider equation (3.5) along the line $A_i \rightarrow Q_0$,

$$(v_i)_{Q_0} = (v_i)_{A_i} \quad , \quad i = 2, 4 \quad (3.6)$$

$$(v_i)_{Q_0} = x_i \quad , \quad i = 1, 3 \quad (3.7)$$

where x_i is the unknown values due to the missing characteristics. Introducing this to (3.3), the following relationship is obtained

$$v_{Q_0} = \begin{pmatrix} x_1 \\ (v_2)_{Q_0} \\ x_3 \\ (v_4)_{Q_0} \end{pmatrix} = TA \begin{pmatrix} y_1 \\ y_2 \\ y_3 \\ y_4 \end{pmatrix} \quad (3.8)$$

Two values of y_i must then be specified in order to complete the system and (3.8) can be solved as a set of four equations and four unknowns. The specific form of the two y_i depends on the system components.

Two sets of boundary conditions were used in the simulations. The upstream boundary has been modeled as a rigidly fixed pipe to a reservoir of constant pressure for both cases. Using the notation from (3.8), this yields

$$y_2 = (P)_{Q_0} = P_{res} \quad , \quad y_3 = (\dot{u}_z)_{Q_0} = 0 \quad (3.9)$$

For the downstream boundary, with the valve closing immediately at $t = 0$, the conditions used are a rigidly fixed valve, giving

$$(V)_{Q_{N+1}} = (\dot{u}_z)_{Q_{N+1}} = 0 \quad (3.10)$$

and an unrestrained valve, giving

$$y_1 = (V)_{Q_{N+1}} = (\dot{u}_z)_{Q_{N+1}} \quad (3.11)$$

$$A_f p - A_s \sigma_z = \pm m \ddot{u}_z \pm c \dot{u}_z \pm k u_z \quad (3.12)$$

Using the former will turn off the junction coupling in the equations. This is the reason it is included here, because comparing the two cases highlights the significance of accurately accounting for the domain coupling in the FSI-investigation of piping systems.

4. Experimental setup

The numerical method explained above is to be validated experimentally using direct measurements of fluid pressure, pipe-wall axial strain and system acceleration. This section will concern the setup and instrumentation, as well as some numerical predictions.

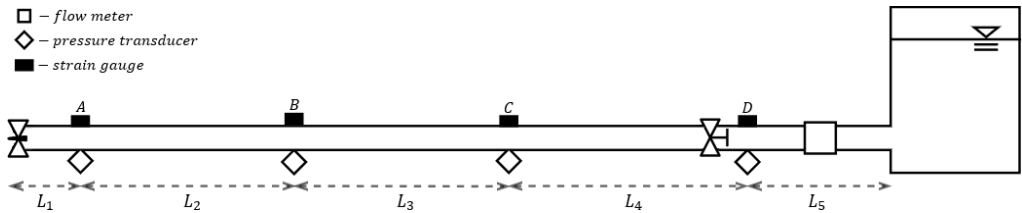


Figure 2: Schematic of the laboratory setup.

$$L = [990 \ 6060 \ 6060 \ 6160 \ 4990] \text{ mm}$$

Table 1: Description of instruments used for the measurements

Variable	Limit	Instrument	Calibration	DAQ Module
Pressure	17 bar	Kulite HKM-375M-17BARA	DPI 601	NI-9237 (Bridge)
Strain	$\pm 5\%$	HBM LY19-10/120A	Shunt calibration	NI-9237 (Bridge)
Acceleration	25 kHz	B&K DeltaTron Type 4397	Factory calibration	NI-9233 (IEPE)

4.1. Setup

A schematic of the experimental apparatus is shown in figure 2. The pipe has a total length $L = 24260$ mm, a inner diameter $D = 100$ mm and a wall thickness $e = 2$ mm. The upstream reservoir is a high pressure tank with a free water surface. The downstream valve is a Pelton nozzle with an outlet diameter of $d = 40$ mm. The upstream valve is a manual butterfly valve in place to shut off the water supply to the pipe when it is not in-use. Furthermore, the pipe is designed to endure an internal pressure of $P_{int} = 10$ bar (abs), which will be limiting for the experiments.

4.2. Instrumentation

Three different variables of interest is to be measured, namely fluid pressure, pipe-wall axial strain and axial acceleration of the system. Additionally, the steady flow rate and nozzle position will be measured to use as references in the validation. The specific types of instruments used are listed in table 1. Placed at each measuring point (A-D) are one pressure transducer, measuring absolute pressure, and one linear strain gage, mounted to measure axial elongation and contraction. Only one accelerometer is used to start with (at position B), to investigate if it is able to produce sensible results.

5. Numerical results and discussion

The experimental setup is modeled with the MOC-procedure described in section 3. The grid consists of four nodes in z-direction and 1333 nodes in time. The ration number for wave velocity adjustment is chosen as $b/a = 30/7$ and the steady state fluid velocity is set to 0.5 m/s.

The different effects from the couplings present in the system can observed from the numerical results above. The Poisson coupling gives the precursor waves. These weaker, faster pressure waves travel through the system, altering the entire behavior. As they travel through the system, they will force the pipe-wall to expand or contract radially as well. This effect gives an exponentially growing amount of pressure waves, traveling at different velocities through the system. This is believed to be the reason for the characteristic behavior of the pipeline parameters through the waterhammer-event.

The other coupling effect, the junction coupling can be observed by comparison of the fixed and free valve-cases shown in figure 3. The fixed valve-case resembles what is known as the classical waterhammer response, with the exception of the high frequency ripples on the crest and in the trough (see figure 3a). The free valve-case gives a completely different response. Since the latter is believed to be the more physically accurate boundary conditions, this highlights the need for well-posed boundary models to get reasonable predictions from the simulations.

When physical processes are modeled mathematically, some simplifications and assumptions will always be necessary. Crucial to the model used here, is the long wave length assumption, making it one-dimensional. It can be observed in figure 3b that the structural oscillations have a significantly higher frequency than the fluid variables. One explanation is the difference in wave propagation velocities, where the stress waves are four times faster than the pressure waves, consequently giving higher frequency oscillations. But nevertheless, the validity of the long wavelength assumption should be questioned.

One other modeling aspect to consider is the friction model. While waterhammer effect are expected to be damped out and disappear, the simulations show no signs of this for prolonged runs. The behavior

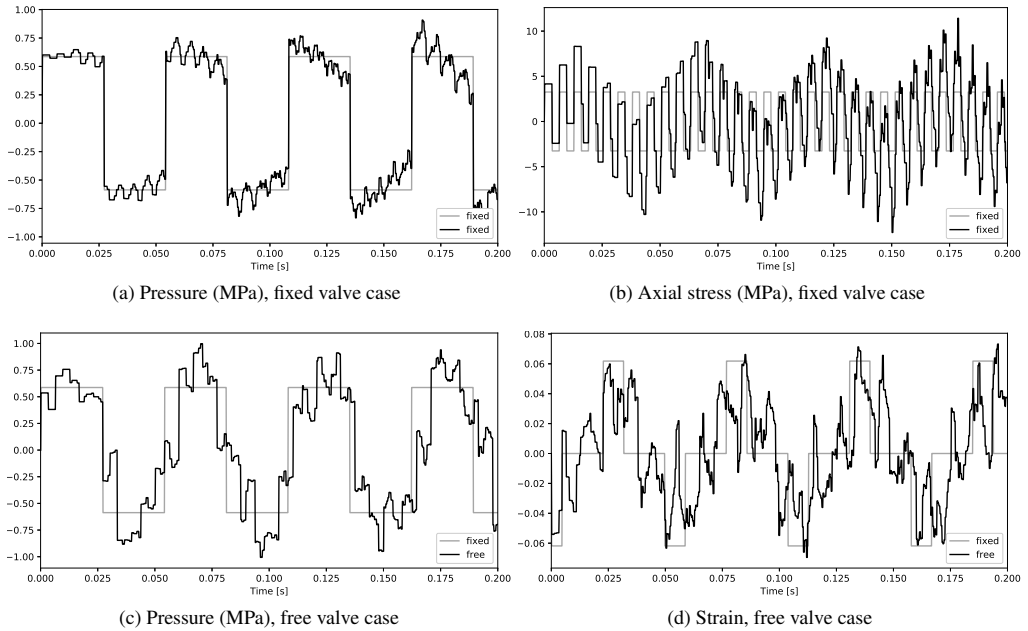


Figure 3: Transient history at valve, coupled (solid line) vs. uncoupled solution (faded line).

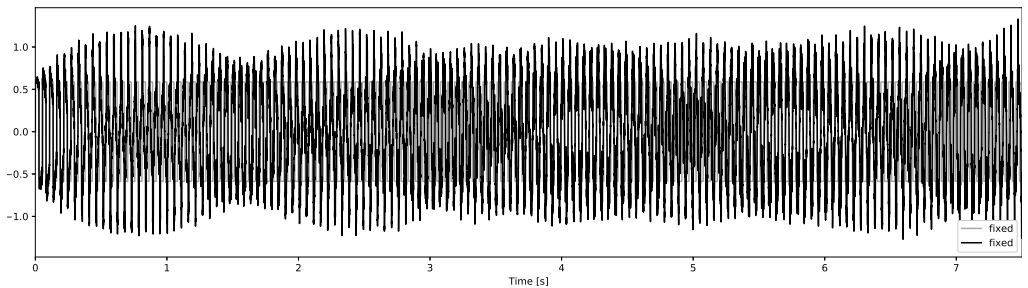


Figure 4: Prolonged simulation results (7.5s), pressure (MPa) at the valve, fixed valve case.

can be observed in figure 4. This is named the Poisson coupling beat in literature and is considered a strictly numerical behavior arising from the model [9, 10]. The source for this lack of physical behavior are suspected to be the steady friction assumption. Adding complexity to the friction model, making it account for unsteadiness, can give a more realistic response and several options exist suited for the present problem.

6. Conclusion

The fluid-structure interaction in a pipe has been investigated using mathematical modeling. Some key aspects for understanding the behavior of the two interconnected domains has been addressed, as well as a MOC-modeling approach for solving a waterhammer-event numerically. This approach has proven

itself suitable for the task, especially with its rapid execution times. The need for accurate models have been identified because of the way both couplings alter the system response. Since some simplifications are necessary in almost all modeling processes, model verification and validation is a must to fully rely on the predictions the numerical model gives. The first results highlight two areas of interest, namely a more complex friction model and verification of the one-dimensional assumption made in deriving the four-equation model.

6.1. Further work

In order to validate the computer code written to solve the equation system, a experimental analysis of a similar reservoir-pipe-valve setup is to be conducted. Presently the apparatus and instrumentation is final stages of completion. During the spring of 2018, measurements will be taken, processed and compared with simulation results for validation purposes. Model verification is also to be addressed, for the purpose of highlighting limitations with the use of the method of characteristics for modeling waterhammer-events. Some work is planned to incorporating a unsteady friction model and non-instantaneous valve-closure in the numerical model.

References

- [1] Topiwala J, Mistry G, Patel S and Umrigar P 2016 *The Int. Jour. of Research in Mech. Engi. & Tech.* **6** 65–8
- [2] Wylie E B and Streeter V L 1993 *Fluid Transients in Systems* (Englewood Cliffs, N.J.: Prentice Hall)
- [3] Tijsseling A S 1993 *Fluid-Structure Interaction in case of Waterhammer with Cavitation, Ph.D Thesis* (Delft University of Tech., The Netherlands: Comm. on Hydraulic & Geotech. Engi.) report No. 93-6
- [4] Nave C R Wave speeds <http://hyperphysics.phy-astr.gsu.edu/hbase/Sound/souspe2.html> 'Georgia State University : Accessed: 05.12.2017
- [5] Williams D J 1977 *Jour. Mech. Engi. Science* **19** 237–42
- [6] Ferziger J and Peric M 2002 *Computational Methods for Fluid Dynamics* 3rd ed (Berlin Heidelberg: Springer-Verlag) ISBN 3-540-42074-6
- [7] Toro E F 2009 *Riemann Solvers and Numerical Methods for Fluid Dynamics* (Berlin Heidelberg: Springer-Verlag) ch. 2, p. 42-85
- [8] Lavooij C S W and Tijsseling A S 1991 *Jour. of Fluids and Structures* **5** 573–95
- [9] Tijsseling A 1997 *4th Int. Symp. on Fluid-Structure Interactions, Aeroelasticity, Flow-Induced Vibration and Noise* **53-2** 529–32
- [10] Ferras D, Covas D I C and Schleiss A J 2017 *Jour. of Hydraulic Research* **55** 491–505